Spatially varying peatland initiation, Holocene development, carbon accumulation patterns and radiative forcing within a subarctic fen

Piilo, Sanna

2020-11-15

Piilo , S , Korhola , A , Heiskanen , L , Tuovinen , J-P , Aurela , M , Juutinen , S , Marttila , H , Saari , M , Tuittila , E-S , Turunen , J & Väliranta , M 2020 , ' Spatially varying peatland initiation, Holocene development, carbon accumulation patterns and radiative forcing within a subarctic fen ' , Quaternary Science Reviews , vol. 248 , 106596 . https://doi.org/10.1016/j.quascirev.2020.106596

http://hdl.handle.net/10138/349660
https://doi.org/10.1016/j.quascirev.2020.106596

Spatially varying peatland initiation, Holocene development, carbon accumulation patterns and radiative forcing within a subarctic fen

Sanna R. Piilo*[a,b], Atte Korhola[a,b], Lauri Heiskanen[c], Juha-Pekka Tuovinen[c], Mika Aurela[c], Sari Juutinen[a,b], Hannu Marttila[d], Markus Saari[d], Eeva-Stiina Tuittila[e], Jukka Turunen[f], Minna M. Väliranta[a,b]

[a] ECRU, Ecosystems and Environment Research Programme, Department of Environmental Sciences, University of Helsinki, P.O. Box 65, 00014, Finland

[b] Helsinki Institute of Sustainability Science (HELSUS), Finland

[c] Finnish Meteorological Institute, Erik Palménin aukio 1, 00560, Helsinki, Finland

[d] Water, energy and Environmental Engineering Research Unit, University of Oulu, P.O. Box 4300, 90014, Finland

[e] School of Forest Sciences, University of Eastern Finland, P.O. Box 111, Joensuu, Finland

[f]Environmental Solutions, Peatland Use and Resource Economics, Geological Survey of Finland, P.O. Box 96, 02151, Espoo, Finland

*Corresponding author: email: sanna.piilo@helsinki.fi

Abstract

High latitude peatlands act as globally important carbon (C) sinks and are in constant interaction with the atmosphere. Their C storage formed during the Holocene. In the course of time, the aggregate effect of the C fluxes on radiative forcing (RF) typically changes from warming to cooling, but the timing of this shift varies among different peatlands. Here we investigated Holocene peatland development, including vegetation history, vertical peat growth and the lateral expansion of a patterned subarctic fen in northern Finland by means of multiple sampling points. We modelled the Holocene RF by combining knowledge on past vegetation communities based on plant macrofossil stratigraphies and present *in situ* C flux measurements. The peatland initiated at ca. 9500 calibrated years Before Present (cal yr BP), and its lateral expansion was greatest between ca. 9000 and 7000 cal yr BP. After the early expansion, vertical peat growth proceeded very differently in different parts of the peatland, regulated by internal and external factors. The pronounced surface microtopography, with high strings and wet flarks, started to form only after ca. 1000 cal yr BP. C accumulation within

the peatland recorded a high degree of spatial variability throughout its history, including the recent past. We applied two flux scenarios with different interpretation of the initial peatland development phases to estimate the RF induced by C fluxes of the fen. After ca. 4000 cal yr BP, at the latest, the peatland RF has been negative (cooling), mainly driven by C uptake and biomass production, while methane emissions had a lesser role in the total RF. Interestingly, these scenarios suggest that the greatest cooling effect took place around ca. 1000 cal yr BP, after which the surface microtopography established. The study demonstrated that despite the high spatial heterogeneity and idiosyncratic behaviour of the peatland, the RF of the studied fen followed the general development pattern of more southern peatlands. Holocene climate variations and warm phases did not seem to induce any distinctive and consistent peatland-scale patterns in C accumulation, whereas our data suggests that the changes in vegetation related to autogenic succession were reflected in the C accumulation patterns and RF more clearly.

Keywords: aapa mire, carbon dynamics, lateral expansion, autogenic succession, paleoecology, vegetation dynamics, climate variation, high latitudes

1. Introduction

Northern peatlands are an important element in the global carbon (C) cycle and act as a C sink, representing ca. 90% of the 545 (475–620) Gt C stored in peatlands globally (Yu et al., 2010), A more recent estimate of the global peatland C store is 1055 Gt C (Nichols and Peteet, 2019). Northern peatlands are globally essential C stores with ca. one third of all soil C stored in them due to the slow decomposition in waterlogged conditions and low temperatures (Gorham, 1991). Due to recent climate change, the C storage accumulated during the Holocene may be compromised. High latitudes are warming at a rate twice the global average (IPCC, 2013), the Arctic has already warmed by 2–3°C since the late 19th century (Post et al., 2019) and precipitation has increased by 6 % during the past ca. 50 years (Box et al., 2019). High uncertainties are especially related to future precipitation (Box et al., 2019; Collins et al., 2013), which will together with the temperature rise, affect peatland moisture conditions and thus vegetation assemblages and C accumulation capacity especially in northern regions (McGuire et al., 2018; Helbig et al., 2020).

Post-glacial peatland initiation in high latitudes overall was triggered by rising growing season temperatures and the availability of excess water (Morris et al., 2018) peaking in the early Holocene 11,000–9000 calibrated years before present (cal yr BP; present = 1950 Common Era (CE)) (MacDonald et al., 2006; Ruppel et al., 2013; Yu et al., 2010). As interpreted from peat archives, Holocene climate variations are reflected in peatland dynamics (Charman et al., 2013; Yu et al., 2009). For example, during the warm Medieval Climate Anomaly (MCA; 1000–700 cal yr BP (Mann et al., 2009)) and Holocene thermal maximum (HTM; 8000–4800 cal yr BP (Renssen et al., 2012)), increased net primary productivity (NPP) exceeded peat decomposition, leading to accelerated peat accumulation (Charman et al., 2013; Yu et al., 2009). In contrast, over the climate transition from the MCA to the Little Ice Age (LIA; 500–100 cal yr BP (Wilson et al., 2016)), C sequestration rates of northern peatlands declined, possibly because of the lower temperatures combined with increased cloudiness, which suppressed NPP (Charman et al., 2013).

Peatlands exchange greenhouse gases (GHG) with the atmosphere, which generates radiative forcing (RF) with climatic implications. A negative (cooling) RF results from net uptake of carbon dioxide (CO_2), while the methane (CH_4) emissions have an opposite (warming) impact associated with positive RF (Frolking and Roulet, 2007; Yu, 2011). In general, peatlands simultaneously sequester and release C, the balance associated with the peatland surface microtopography (Alm et al., 1999; Waddington and Roulet, 2000). During its succession, a peatland may act as both a C sink and a source, depending on various autogenic and allogenic forcing factors (Korhola et al., 1996; Yu, 2011). While the net RF depends on the balance between CO_2 and CH_4 fluxes, it is important to note that these two gases differ greatly in their radiation efficiency and residence time in the atmosphere (Myhre et al., 2013). Therefore, the initial net RF effect of a newly

developed peatland is mainly warming, due to the dominance of CH_4 emissions. Over the course of time, however, the negative RF due to sustained CO_2 sequestration exceeds the CH_4 –induced positive forcing, which leads to a negative net RF, i.e. cooling effect (Frolking and Roulet, 2007; Mathijssen et al., 2014).

The Holocene C dynamics of subarctic permafrost-free fens have received less attention (Juutinen et al., 2013; Mäkilä et al., 2001; Mäkilä and Moisanen, 2007; Mathijssen et al., 2014) than the C dynamics of permafrost peatlands (e.g. Gałka et al., 2018; Pelletier et al., 2017; Sannel et al., 2017; Zhang et al., 2018a) or boreal bogs (e.g. Korhola et al., 1996; Mathijssen et al., 2016; Turunen et al., 2001; Van Bellen et al., 2011). Fens, however, respond to changes in the environment, especially moisture conditions, more strongly and faster than bogs (Gong et al., 2013; Jaatinen et al., 2007; Kokkonen et al., 2019; Tahvanainen, 2011; Wu and Roulet, 2014). Moreover, a pronounced decline in C accumulation over the warm and dry mid-Holocene climate phase (ca. 8000–5000 cal yr BP (e.g. Eronen et al., 1999; Seppä et al., 2009)) has been recorded for subarctic fens (Mäkilä and Moisanen, 2007; Mathijssen et al., 2014; Robinson, 2006). This contradicts the patterns reported by Yu et al. (2009) for northern peatlands, where an overall slowdown of C accumulation after 4000 cal yr BP was connected to climate cooling following the high accumulation rates during the warm mid Holocene. As motivated by the current highly pronounced warming in the subarctic region, there is a need to deepen our understanding of the connections between climate and the ecosystem processes, C dynamics and atmospheric forcing of subarctic fens.

Here, we aim to link the long-term history of the subarctic Kaamanen peatland to its present-day C dynamics. To contribute to the understanding of the future peatland-climate interactions and scenarios, we explored how the Holocene warm climate phases, i.e. HTM, MCA and recent warming since the 1980s, are reflected in peatland physical and biological dynamics and what was the consequent radiative forcing effect. To reconstruct C flux dynamics since the peatland initiated we combined paleoecological data with contemporary measurements, and took advantage of the present-day GHG flux measurements conducted at the site and within its catchment. At the site, the ecosystem-atmosphere exchange of CO_2 has been measured using the eddy covariance (EC) technique since 1997 (Aurela et al., 2004, 2002, 2001, 1998), and plant community specific GHG fluxes have been measured by chambers (Maanavilja et al., 2011; Heiskanen et al. 2020). Under the current climate conditions, the peatland is a weak C sink of ca. -20 g C m^{-2} yr^{-1} on average (Aurela et al., 2004; Hargreaves et al., 2001; Heiskanen et al. 2020). Reconstruction of the peatland development history, initiation and subsequent lateral expansion, allowed us to use these flux data to model the RF of the fen from its initiation to the present.

2. Material and methods

2.1 Site description

Our study peatland (Kaamanen, 69° 8.44′ N, 27° 16.19′ E, 155 m a.s.l.) is a subarctic patterned flark fen (ca. 43 ha) characteristic of the northern aapa mire region (Figure 1). The long-term (1981–2010 CE) mean annual air temperature and precipitation sum are -0.4°C and 472 mm, respectively (Pirinen et al., 2012). Direction of water flow is from north to south, and spring flooding is typical. Strings (hummocks) and flarks (hollows) with a dimension of few metres create a patterned mosaic of surface microtopography. Ombrotrophic strings are typically lower than 1 m, but extend clearly above the surrounding water table, and can remain frozen inside until late summer (Maanavilja et al., 2011). The Kaamanen peatland is located within the sporadic permafrost zone, the so-called palsa mire zone (Figure 1), but has no permafrost. The inundated flarks close to a small stream, lining the east of the studied fen area, are mesotrophic. The prevailing vegetation varies greatly among different parts and microtopographic features of the fen. Flark vegetation is mainly composed of sedges *Carex spp., Trichophorum cespitosum* and *Eriophorum angustifolium,* the forb *Menyanthes trifoliata* and brown mosses (typically *Scorpidium scorpioides*). Tall sedge vegetation fringes the stream. Strings are dominated by forest and hummock mosses such as *Dicranum spp.* and *Pleurozium schreberi,* lichens, and *Rhododendron tomentosum, Empetrum nigrum, Vaccinium uliginosum, V. vitis-idaea* and *Rubus chamaemorus. Andromeda polifolia, Betula nana* and *Salix spp*. and peat mosses (*Sphagnum fuscum* and *S. capillifolium)* are found at the margins of the strings (Maanavilja et al. 2011). Wet lawns with *S. lindbergii* and low hummocks characterised by *S. fuscum* and dwarf shrubs dominate the south-west part of the study area. *Pinus sylvestris* forest and small lakes surround the peatland. Peat thickness in the northern part of the fen is ca. 1 m, but in the south, closer to the lake, it is up to 4 m (Figure 1).

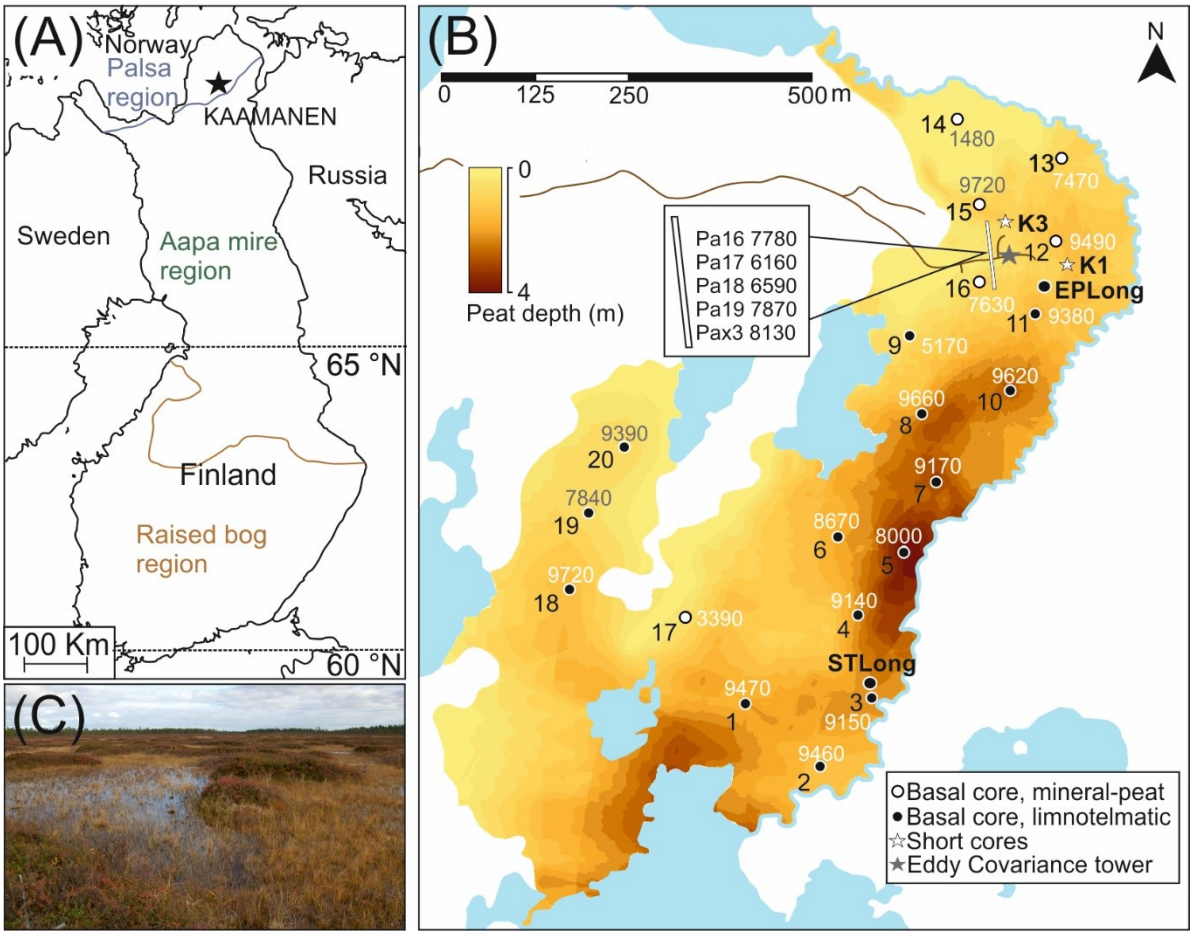

Figure 1. Study area located in northern Finland (A). The black star shows the location of the study site and the coloured lines indicate the distribution of raised bogs (ombrotrophic peatlands), aapa mires (peatland complexes with minerotrophic fen conditions in the central parts) and palsa peatlands (fens with frozen peat mounds) in Finland. (B) Isochrone map of the studied peatland area and the peat thickness. Coring locations are shown with dots and white stars with the number or the name of the location and calibrated basal ages (cal yr BP). White line with Pa –codes indicates a coring transect. (C) The microtopographic variation of flarks and strings.

2.2 Peat thickness measurement and sampling

We selected the coring locations based upon a ground-penetrating radar (GPR, Malå GeoScience ProEx) survey of the peat thickness and the underlying topography, conducted during the snow cover period in April 2018. The total length of measurement transects was 9.6 km which were measured using a snowmobile to pull the antennae (50 MHz, approximate velocity 5 m s^{-1}). The measurement transects and the data analysis were performed using the ReflexW (Version 8.0, Sandmeier, 2016) programme. Measured subsoil, peat and sediment thickness data were used as validation of the radar data.

To address initial and long-term development, twenty basal peat samples, representing the first peat deposited upon the top of the minerogenic sediment were collected with a Russian peat corer (3 x 50 cm). A long core recovered from a location where the current surface vegetation comprises *Sphagnum-Trichophorum* (STLong 393 cm) was collected in September 2018 and a second long core was recovered from a microform where Ericales-*Pleurozium* comprise the surface vegetation at the crest of a string (EPLong 228 cm) in 2010 (Figure 1). An additional short transect of basal samples was collected in 2009 from the northern part of the peatland (Figure 1). To address more recent development, an additional four short cores were collected with a box corer (7 x 4 x 65 cm) in September 2016. To cover the spatial variability, the short cores were collected from string margins with *Betula-Sphagnum* vegetation (K1BS, K3BS) and from the dry strings (K1EP, K3EP) with Ericales-*Pleurozium* vegetation. Short cores were collected from the northern part of the peatland, where the surface microtopography is more pronounced. Cores were wrapped in plastic and transported, avoiding compaction, inside plastic tubes to the University of Helsinki. Cores were cut to 1 or 2 cm slices and the subsamples were stored in plastic bags at 6 °C.

2.3 Plant macrofossil analysis

Plant macrofossil analysis was conducted to detect and to reconstruct changes in vegetation assemblages. In the short cores, the analysis was performed at 2 cm resolution and in the EPLong long core at every 10 cm and in STLong core at every 20 cm. Volumetric samples (5 ml) were inspected following Mauquoy and van Geel (2007) as modified by Väliranta et al. (2007). Samples were rinsed with water using a 140-µm sieve and the residue was analysed for proportions of main peat components. A stereomicroscope was used to estimate percentages for the total sample volume and a light microscope for further species level identification (for identification: e.g. Laine J. et al. 2009; Eurola et al. 1992 and a reference collection at the University of Helsinki). Seeds and leaves were counted as exact numbers (Figure A.1). Percentage of unidentified organic material (UOM) was estimated if the organic remains were unidentifiable for the vegetation type. Diagrams were created using software C2 (Juggins, 2007) and Tilia 2.0.41 (Grimm, 1991).

2.4 Chronology

A total of 33 samples were sent for accelerator mass spectrometry (AMS) ^{14}C analysis to the Poznan Radiocarbon Laboratory (Poznan, Poland), 19 samples to the Finnish Museum of Natural History (LUOMUS, Helsinki, Finland) and 3 samples were dated in the A. E. Lalonde AMS Laboratory (University of Ottawa) (Tables A.1 and B.1). Either bulk peat, cleaned from rootlets (Holmquist et al., 2016), or identified plant macrofossils were selected for dating (Table B.1). Basal samples were ^{14}C dated to reconstruct the lateral expansion of the peatland following the procedure introduced in Korhola (1994). To depict changes in vegetation type, two long cores and four short surface cores were

157 ^{14}C dated. The two long cores taken from a wet *Sphagnum – Trichophorum* flark (STLong) and dry Ericales –
158 *Pleurozium* string (EPLong) were dated only by ^{14}C. For both long cores, basal ages from the nearest basal peat
159 sampling points, a few tens of metres away, were used instead of the original bottom-most ages of the cores, because
160 the obtained ages show inconsistencies with different materials dated. Dated *Equisetum* remains provided consistently
161 younger ages than selected terrestrial plant macrofossils (*Carex* spp. seeds, *Betula* seeds, *Potentilla palustris* seeds,
162 *Salix* sp., bark and woody remains) (Table B.1) (Howard et al., 2009; Väliranta et al., 2014). For the STLong, the
163 bottom-most age was from a basal peat sample from the coring point 3 and for EPLong from coring point 11 (Figure 1).
164 The four surface cores were additionally ^{210}Pb dated at the University of Exeter, UK, using alpha-spectrometry at 2 cm
165 intervals. 0.2−0.5 g of dried and ground peat from each depth were analysed and spiked with a ^{209}Po yield tracer (Kelly
166 et al., 2017; Estop-Aragonés et al., 2018 for the method). The Constant Rate of Supply model (CRS) was applied to
167 obtain the ^{210}Pb ages (Appleby and Oldfield, 1978). Age-depth models (Figure 2), combining both the ^{14}C results and
168 ^{210}Pb dates were created with BACON v2.3.3 package (Blaauw, 2010; Blaauw and Christen, 2011) in R version 3.4.3
169 (R Development Core Team 2016).

170 *2.5 Peat properties and C accumulation*

171 To determine dry bulk density (g cm^{-3}) of the subsamples, we measured the dry mass (g) of peat based upon a fresh
172 volume of 5 cm^3. For the short cores, C and nitrogen (N) content at 4 cm intervals was measured using a LECO TruSpec
173 micro Elemental Determinator, at the University of Helsinki, and these results were applied to calculate average values
174 for the layers between the measurements. For the two long cores, loss on ignition (LOI) was measured at 10 cm intervals,
175 following Heiri et al. (2001) and C content was estimated assuming 50% of C in organic matter (LOI x 0,5) (Loisel et al.,
176 2014). Apparent C accumulation rates (CAR, g C m^{-2} yr^{-1}) were calculated by multiplying the C mass of each 1 cm
177 increment (g m^{-3}) by the corresponding peat growth rate (m yr^{-1}) (Tolonen and Turunen, 1996), derived from the age-
178 depth models (Figure 2).

179 *2.6 Annual CO_2 and CH_4 balances*

180 In order to model the RF due to peatland development at Kaamanen, we estimated the ecosystem-atmosphere exchange
181 of CO_2 and CH_4 for different vegetation assemblages based on present-day flux measurements. These assemblages were
182 classified as aquatic ('Sandy *Equisetum'*), *Equisetum*-dominated fen communities ('Peaty *Equisetum',* i.e. on organic
183 sediments), non-patterned fens and their composites, which occurred during different development phases before the
184 present patterned fen phase. We reconstructed the successional development areas for these different paleovegetation
185 types. For estimating the paleovegetation types and the timing of the main changes, we applied dating results (Tables A.1

and B.1, Figure 2) and the reconstructed vegetation history, interpreted from plant macrofossils, and extrapolated the changes to the surrounding areas (Figure 1). QGIS (3.0.0) was used to measure the estimated non-overlapping areas of each paleovegetation assemblage on 1000-yr intervals. The flux measurements were made both with the eddy covariance (EC) and chamber techniques, the former providing areally averaged and the latter plant-community-specific data. To calculate the mean annual flux densities (Table 1), the measurement time series were first gap-filled either based on empirical response functions, with temperature and irradiance as the key explanatory variables, or using linear interpolation (Aurela et al., 2002; Juutinen et al., 2013; Laine A. et al., 2009).

Table 1. Flux densities (g C m^{-2} yr^{-1}) adopted for different peatland vegetation assemblages and used for the radiative forcing modelling. Values for "non-patterned fen" are obtained from *Trichophorum* and of *Carex-Scorpidium* dominated surface measurements. "Patterned fen" represents the current peatland spatially averaged estimate based on the EC data. * Values from Juutinen et al. (2013).

	Flux density (g C m^{-2} yr^{-1})		
	CO_2	CH_4	CO_2+CH_4
Sandy *Equisetum**	-10	-0.4	-10
Peaty *Equisetum**	18	5	23
Mix of non-patterned fen & Peaty *Equisetum*	-15	7	-8
Non-patterned fen	-48	8	-39
Patterned fen	-18	6	-12

The EC data (Aurela et al., 2004; Heiskanen et al., 2020) were used for the latest phase, i.e. the past 1000 yr, when the peatland has exhibited pronounced microtopographical heterogeneity and been dominated by four vegetation habitats: (1) *Trichophorum* tussock flarks, (2) wet *Carex-Scorpidium* flarks, (3) *Sphagnum-Betula nana* string margins and (4) Ericales-*Pleurozium* string tops, defined in Maanavilja et al. (2011). The areal coverage of these habitats was determined by drone imaging with very high spatial resolution within a 200-m radius from the EC measurement tower (Räsänen et al., 2019). The EC data cover eight years for both CO_2 (1997–2002, 2017–2018) and CH_4 (2011–2018) fluxes.

Both EC measurements and flux chamber data of the *Trichophorum* and *Carex-Scorpidium* communities (Heiskanen et al., 2020) were used to reconstruct the past C exchange of the Cyperaceous fen during a phase when the present

207 microtopographical features were not yet developed. During the growing season, the relative difference between the
208 EC- and chamber-based data was used to scale the chamber-based CO_2 fluxes to match the EC fluxes separately for the
209 ecosystem respiration and gross primary production estimated from the data (Aurela et al., 2002; Heiskanen et al.,
210 2020). Outside the growing season, the EC-based CO_2 fluxes were allocated proportionally to the *Trichophorum* and
211 *Carex-Scorpidium* communities based on the respiration fluxes measured with chambers during the last two weeks of
212 the growing season. The annual ecosystem-scale CH_4 balance was partitioned to these plant communities similarly to
213 the CO_2 balance, i.e. the EC data were allocated according to the chamber-based plant-community-specific fluxes. An
214 equal areal coverage of *Trichophorum* and *Carex-Scorpidium* communities was assumed for the flux reconstruction.

215 In addition to the local fluxes, we included flux data measured with chambers (year around estimate complemented by
216 snow-gradient measurements) across the Kiposuo peatland – Kipojärvi lake continuum, located within the same
217 catchment ca. 6 km northeast of Kaamanen (Laine A. et al., 2009; Juutinen et al., 2013). These data represent aquatic
218 vegetation communities in shallow water conditions (*Equisetum fluviatile*, mixed *E. fluviatile* and *Carex* spp.) and were
219 here adopted for an early *Equisetum*-limnotelmatic phase of the study peatland. Two different vegetation types were
220 included: (1) littoral vegetation patches on sandy sediments ('Sandy *Equisetum*'), with net uptake of C, and (2) littoral
221 vegetation on organic sediments ('Peaty *Equisetum*'), with net release of C.

222 These two data sets make it possible to assess how the likely release of excess CO_2 from the peatland-lake ecotone to
223 the atmosphere affects the RF simulation. In other words, we assumed that the current peatland, at places where it
224 developed from a limnic system, has been a temporary net C source due to release of CO_2 from the net heterotrophic
225 littoral zone.

226 Two alternative simulation scenarios were outlined for the *Equisetum* fluxes. In Scenario 1, we used the flux
227 measurements from the 'Sandy *Equisetum*' habitat for the earliest phase of the peatland, since underneath the paleo-
228 vegetation layer lies mineral ground and thus this paleo-habitat resembles littoral sand conditions. For the peatland
229 development phases following this, we adopted 'Peaty *Equisetum*' as the representative habitat. In Scenario 2, we used
230 the fluxes from littoral sand for the first 1000 yr and linearly interpolated between them and the fluxes of 'Peaty
231 *Equisetum*' for the following four millennia, assuming that this represents the change from littoral conditions to peat-
232 forming vegetation. For the vegetation assemblage 'Mix of non-patterned fen and Peaty *Equisetum*', inferred from the
233 plant macrofossil analysis, we used the average of the corresponding fluxes.

234 ### 2.7 *Radiative forcing modelling*

235 The areas of different vegetation assemblage classes defined above and listed in Table 1, were multiplied by the
236 corresponding flux densities (g m^{-2} yr^{-1}) (Table 1) to obtain the total CO_2 and CH_4 fluxes (g yr^{-1}) for the Kaamanen
237 peatland during each 1000-yr slot from 10,000 cal yr BP to the present. These fluxes were used as input to the calculation
238 of radiative forcing, i.e. the change in Earth's radiative balance due to the perturbations to atmospheric GHG
239 concentrations that resulted from peatland development. RF was calculated in annual time steps with a sustained impulse-
240 response model (Lohila et al., 2010; Mathijssen et al., 2017).

241 CO_2 and CH_4 are long-lived GHGs that can be assumed to be instantaneously and completely mixed in the atmosphere
242 (Myhre et al., 2013). Therefore, the atmospheric composition change due to surface exchange fluxes of these GHGs, even
243 if occurring at a local scale, was calculated in the RF model simply as a change in the total mass of each GHG assuming
244 globally uniform concentration distribution. Uptake fluxes were treated as negative emissions.

245 The atmospheric GHG pulses were modelled to decay according to characteristic time scales related to the global
246 biogeochemical cycles of each GHG (Frolking et al., 2006). For CO_2, this was implemented as a weighted sum of four
247 exponential functions, where the fastest perturbation time scale was 4.3 yr and the slowest decay effectively corresponded
248 to a permanent atmospheric change for 22% of each annual pulse. This impulse–response function for CO_2 decay was
249 derived by Joos et al. (2013) from a multi-model ensemble of simulations with coupled carbon cycle–climate models.
250 The corresponding function for CH_4 was defined as a first-order decay with a single perturbation time scale of 12.4 yr
251 (Myhre et al., (2013), i.e. a short-term atmospheric response to CH_4 emission in comparison to CO_2 uptake.

252 The annual emission pulses were integrated in such a way that in each year the effect of all preceding pulses and their
253 decay with time was accounted for in the atmospheric GHG concentration change. As a major part of the CH_4 decay
254 results from atmospheric oxidation of the emitted CH_4 molecules to CO_2, this conversion was included in the RF model.
255 The additional CO_2 generates an indirect RF effect that was allocated to the CH_4 emissions. An efficiency of 80% was
256 assumed for the CH_4-to-CO_2 conversion (Boucher et al., 2009).

257 The instantaneous RF (W m^{-2}) resulting from the modelled CO_2 and CH_4 concentration changes was calculated with a
258 radiative efficiency parameterization that was derived by Etminan et al. (2016) from simulations with a detailed radiation
259 transfer model. These parameterizations relate the RF of each GHG to the concentration change taking into account the
260 spectral interactions between the key GHGs, i.e. CO_2, CH_4 and nitrous oxide (N_2O). The RF due to peatland fluxes was
261 calculated as a marginal change with respect to a specified background concentration (Lohila et al., 2010). The variation
262 of background concentrations of CO_2, CH_4 and N_2O during the Holocene was adopted from Köhler et al. (2017).

263 **3. Results**

3.1 Age-depth models and peat growth rates

Peat growth rate in EPLong (Ericales – *Pleurozium* string), was, on average, 0.2 mm yr^{-1} from ca. 9270 cal yr BP (227 cm) to ca. 95 cal yr BP (43 cm). The average and the highest peat growth rates in STLong (*Sphagnum* – *Trichophorum* flark) were 0.4 and 0.6 mm yr^{-1} (between ca. 8330 cal yr BP (325 cm) and 6070 cal yr BP (190 cm)), respectively (Figures 2 and 3).

Based on the established age-depth models using ^{14}C and ^{210}Pb dating results, peat growth rates had not been constant during the shorter time scale either (Figures 2 and 4). For K1EP, the peat growth rate was fast between ca. 1290 (58 cm) and ca. 1050 (30 cm) cal yr BP, on average 1.2 mm yr^{-1}. Between ca. 1050 and ca. 120 cal yr BP, peat growth rates slowed down to an average of 0.2 mm yr^{-1} and then accelerated to 1.1 mm yr^{-1} to the present day (figure 2). For K1BS, average peat growth rate was first 0.5 mm yr^{-1} (from ca. 1980 (57 cm) to 1420 (30 cm) cal yr BP) and then decreased to an average of 0.09 mm yr^{-1} (until ca 270 cal yr BP (20 cm)). Towards the surface, the average peat growth rate increases to 0.7 mm yr^{-1} (ca. -60 cal yr BP (5 cm)) and for the top-most layers it reached 6 mm yr^{-1}.

For the K3 short cores, peat growth rates were more consistent over time than in the K1 short cores and showed two distinct phases of low and higher rates (Figures 2 and 4). For K3EP, a low average peat growth rate of 0.2 mm yr^{-1} was detected between ca. 1270 (59 cm) and ca. 450 (40 cm) cal yr BP, after which the peat growth rate increased to 0.8 mm yr^{-1} lasting until the present. For K3BS, the low average peat growth rate phase of 0.1 mm yr^{-1} started from ca. 2690 cal yr BP (57 cm) and lasted until ca. 370 cal yr BP (35 cm), followed by an average peat growth rate of 1.6 mm yr^{-1} with higher rates in the top-most layers.

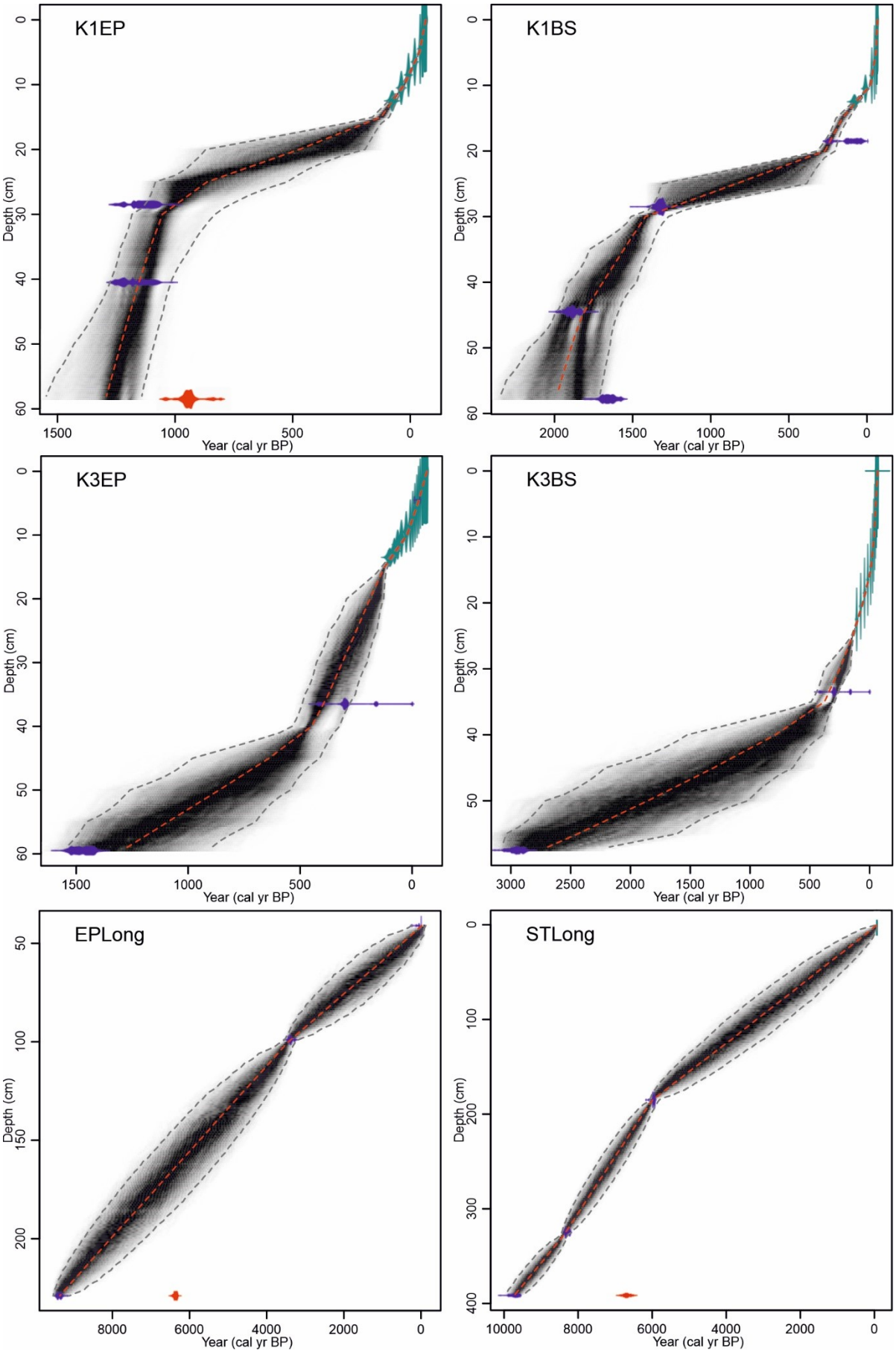

282

Figure 2. BACON derived age-depth models. In green: ^{210}Pb age-ranges (for K1 and K3 cores), and in violet: ^{14}C dates (cal yr BP). The grey shading with the darkest grey demarks most likely age-range and the thin red line shows the weighted mean age based on the model. In red are ^{14}C outliers (K1EP, EPLong and STLong). Notice the differences in the x and y-axis scales.

3.2 Plant community changes and peat properties

STLong: The early assemblages dated to ca. 9500 cal yr BP contained remains of aquatic taxa such as *Charophyta* oospores and *Nymphaeaceae* together with wet indicating bryophytes. After the initial aquatic state, *Equisetum* and Cyperaceae with some woody remains dominated the plant community (Figure 3, Figure A1). *Menyanthes trifoliata*, *Potentilla palustris* and *Potamogeton* seeds were detected at ca. 8650 cal yr BP (340 cm) with some *Sphagnum teres*. Between ca. 9640 to 6360 cal yr BP (388–207.5 cm) the organic content (LOI) varied between 40% and 74%. Between ca. 6230 and 3850 cal yr BP (200–120 cm) the peat forming vegetation was a mixture of *Equisetum* and Cyperaceae. From ca. 6200 cal yr BP (197.5 cm), organic content sharply increased with a marked decrease in peat dry bulk density. Organic content varied between 86% and 97% (characteristic for sedge-dominated peat) to the top of the core with a decrease in dry bulk density towards the surface (Figure 3). After ca. 4490 cal yr BP, the vegetation changed towards fen vegetation mainly composed of Cyperaceae such as *Carex* spp. *Eriophorum* sp. prevailed between ca. 1220 and 570 cal yr BP (40 cm and 20 cm). Sedges and *Sphagnum warnstorfii* dominated the surface. The average dry bulk density was 0.14 g cm^{-3}.

EPLong: The assemblage was first dominated by *Equisetum* remains with some Cyperaceae and woody remains (Figure 3, Figure A.1), mineral material was also abundant. LOI first fluctuated between ca. 9270 and 8000 cal yr BP with values ranging from 43% (199 cm) to 85% (209 cm) (Figure 3). After ca. 8000 cal yr BP (199 cm), LOI values stayed high between 74% and 95%, typical for fen peat. Between ca. 8960- 6200 cal yr BP (220–160 cm) *Menyanthes trifoliata* and *Potentilla palustris* seeds were present. *Carex* spp. seeds and *Betula nana* remains were abundant from ca. 7580 to 3430 cal yr BP (190–100 cm). Roughly, after 7070 cal yr BP (179 cm), vegetation composition became dominated by Cyperaceae with occasional *Sphagna* and other bryophytes. *Equisetum* remains disappeared after ca. 3380 cal yr BP (99 cm). *Eriophorum vaginatum* remains appeared around 3430 cal yr BP and were present until ca. 1060 cal yr BP (100–60 cm). *Sphagnum fuscum* and *S. warnstorfii* dominated the top part, which was not inspected in further detail, from 40 cm (ca. -20 cal yr BP). Relatively even dry bulk density values were observed throughout the core with an average of 0.17 g cm^{-3}. Dry bulk density slightly decreased towards the surface of the core, i.e. during the last ca. 150 years.

K1EP and K3EP (string top sections): Both sites experienced a change from wetter fen vegetation to dry string conditions: K1EP at ca. 1020 cal yr BP and K3EP at ca. 430 cal yr BP (Figure 4, Figure A.1), i.e. there was a 600-year

313 difference between the two sites only ca. 100 metres away from each other. In K1EP, the plant assemblage of the wet fen
314 phase was highly humified (high proportion of UOM) Cyperaceae peat with *Eriophorum* starting from ca. 1290 cal yr BP
315 (58 cm). After ca. 1020 cal yr BP (29 cm), plant composition changed to dwarf shrub roots, bark and leaves. At ca. 90 cal
316 yr BP (13 cm), *Hylocomium splendens* and *Dicranum fuscenscens* emerged. In the top-most 5 cm, *Empetrum nigrum*
317 leaves were abundant. The wet fen section of the K3EP profile was also dominated by Cyperaceae (from ca. 1270 cal yr
318 BP, 59 cm) with *Betula* periderm. The plant assemblages changed through a *Betula-Sphagnum* string margin type (ca.
319 430 cal yr BP, 39 cm) into Ericales-*Pleurozium* string top vegetation (ca. 290 cal yr BP, 28 cm) with dwarf shrub roots
320 and *Hylocomium splendens* and *Pleurozium schreberi*. *Betula nana* and Ericales leaves and bud scales were abundant
321 from the *Betula-Sphagnum* string margin phase throughout the string vegetation development. Average dry bulk density
322 for both string top sections was 0.16 g cm^{-3}. Bulk densities decreased towards the surface taking place between ca. 400
323 and 100 cal yr BP. The centennial-scale declining trend was less pronounced in the string top K1EP, where a decrease
324 occurred only during the recent decades (Figure 4).

325 **K1BS and K3BS** (string margin sections): String margins showed similarities in the changes of plant assemblages and
326 in the timing of the changes. K1BS core was first (ca. 1980 cal yr BP, 57 cm) dominated by Cyperaceae with *Eriophorum*
327 *vaginatum* and *Carex.* From ca. 1820 cal yr BP (45 cm) to ca. 1190 cal yr BP (28 cm) *Sphagnum* section Acutifolia
328 dominated and *Andromeda polifolia* seeds were found (Figure 4, Figure A.1). *Eriophorum vaginatum* was dominant for
329 a ca. one-hundred year period (28–27 cm) and *Empetrum nigrum* leaves were present. *Sphagnum fuscum* dominated
330 between ca. 380 and 90 cal yr BP (21–13 cm). A species composition which is typical for string top vegetation i.e., dwarf
331 shrub roots, *Dicranum* sp. and *Pleurozium shreberi* was abundant between ca. 50 and -60 cal yr BP (12–5 cm), after
332 which the plant assemblages returned to *S. fuscum* domination until the surface of the core. K3BS was at first dominated
333 by Cyperaceae (*Carex* spp. and *Eriophorum vaginatum*) and *Scorpidium scorpioides* from ca. 2690 (57 cm) until ca. 380
334 cal yr BP (35 cm). At ca. 350 cal yr BP (34 cm), the plant assemblage changed and was dominated by *S. fuscum* and *S.*
335 *capillifolium*, but towards the surface was solely *S. fuscum* dominated. Dwarf shrub roots and leaves were also found.
336 Average dry bulk density for both string margin sections was 0.11 g cm^{-3}. Bulk densities decreased towards the surface
337 between ca. 600 and 450 cal yr BP.

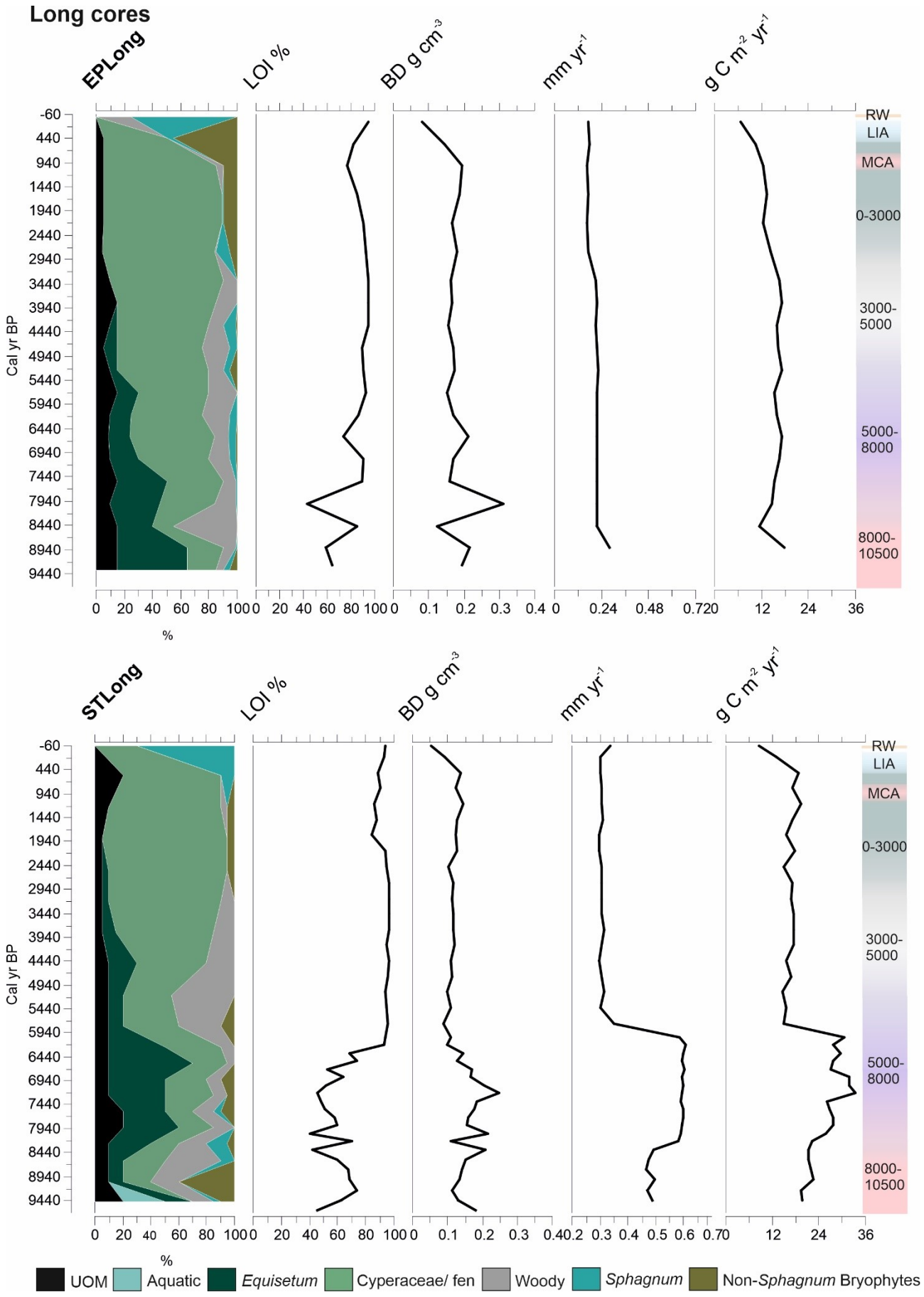
Long cores
EPLong
LOI %
BD g cm-3
mm yr-1
g C m-2 yr-1
Cal yr BP
-60
440
940
1440
1940
2440
2940
3440
3940
4440
4940
5440
5940
6440
6940
7440
7940
8440
8940
9440
RW
LIA
MCA
0-3000
3000-5000
5000-8000
8000-10500
0 20 40 60 80 100
0 20 40 60 80 100
0 0.1 0.2 0.3 0.4
0 0.24 0.48 0.72
0 12 24 36
%
STLong
LOI %
BD g cm-3
mm yr-1
g C m-2 yr-1
Cal yr BP
0 20 40 60 80 100
0 20 40 60 80 100
0 0.1 0.2 0.3 0.4
0.2 0.3 0.4 0.5 0.6 0.7
0 12 24 36
%
UOM
Aquatic
Equisetum
Cyperaceae/ fen
Woody
Sphagnum
Non-Sphagnum Bryophytes

338

Figure 3. Abundance of selected vegetation assemblages (%). Organic content as loss on ignition (LOI%), dry bulk density (BD g cm^{-3}), peat growth rate (mm yr^{-1}), apparent C accumulation rate (g C m^{-2} yr^{-1}). Climate phases (approximate cal yr BP), Recent warming (RW), Little Ice Age (LIA) and Medieval Climate Anomaly (MCA) are indicated with different colours. Red and purple colours indicate warmer and grey, green and blue cooler climate phases. Gradual changes of the climate phases are reflected by shaded colour changes.

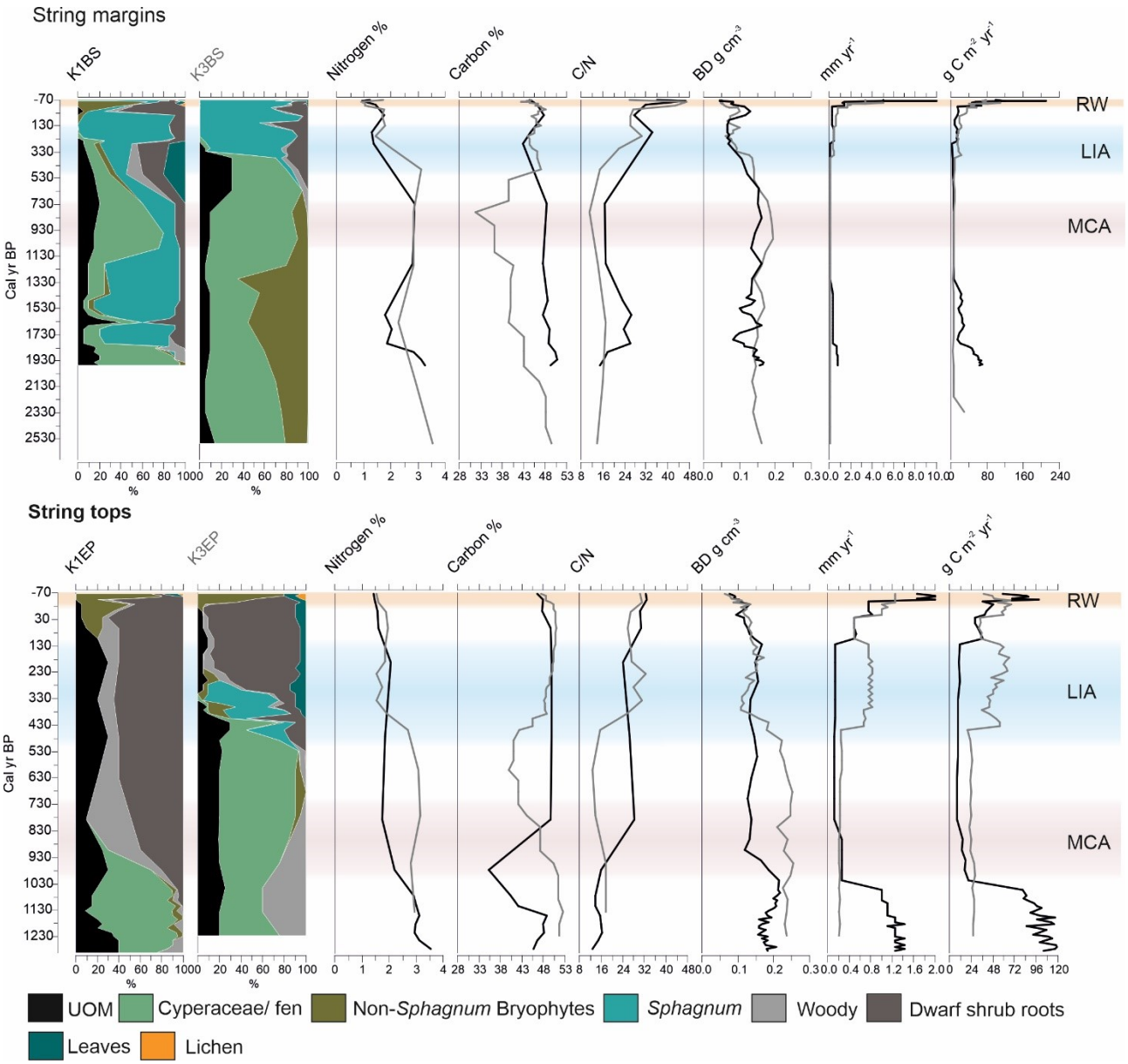

Figure 4. Short string margin records K1BS, K3BS and string top records K1EP, K3EP. Abundance of selected vegetation assemblages (%). Black lines for K1 and grey lines for K3 records. Organic content as loss on ignition (LOI%), dry bulk density (BD g cm^{-3}), peat growth rate (mm yr^{-1}), apparent C accumulation rate (g m^{-2} yr^{-1}). Climate phases (approximate cal yr BP) are indicated with different colours: Recent warming (RW) with orange, Little Ice Age (LIA) with blue and Medieval Climate Anomaly (MCA) with red.

3.3 Plant community changes and lateral expansion through peatland development

In addition to the four community types of the prevailing vegetation inside the EC footprint, we identified three other plant community types from the historical assemblages. Peat started to form in the basin ca. 10,000 cal yr BP (Figure 5). Based on plant macrofossil analyses and sediment properties overall, the southern part of the present peatland area represented an aquatic habitat in the beginning. Limnotelmatic *Equisetum fluviatile* dominated vegetation prevailed in the middle section, but in a small ca. 2.5 ha area in the north, peat started to form directly on top of the mineral soil (Figure 5). Between ca. 9000 and 8000 cal yr BP aquatic habitats changed to *Equisetum* - Cyperaceae dominated habitats and the total area of the peatland increased from 27 ha and to 31 ha (Figure 5). Between ca. 5000 and 4000 cal yr BP the peatland extent was ca. 40 ha. *Equisetum* habitats disappeared after ca. 4000 cal yr BP, after which Cyperaceous fen habitats dominated the entire peatland for ca. 3000 years. The northernmost part of the peatland established via primary paludification which took place ca. 2000 cal yr BP. Young and shallow peat was also found in the south, close to the basal peat coring point number 17, where the peat initiated between 4000 and 3000 cal yr BP. Peat area reached the current 43 ha between ca. 2000 and 1000 cal yr BP. Surface microtopography with high strings and wet flarks formed after ca. 1000 cal yr BP creating the present day strongly patterned features.

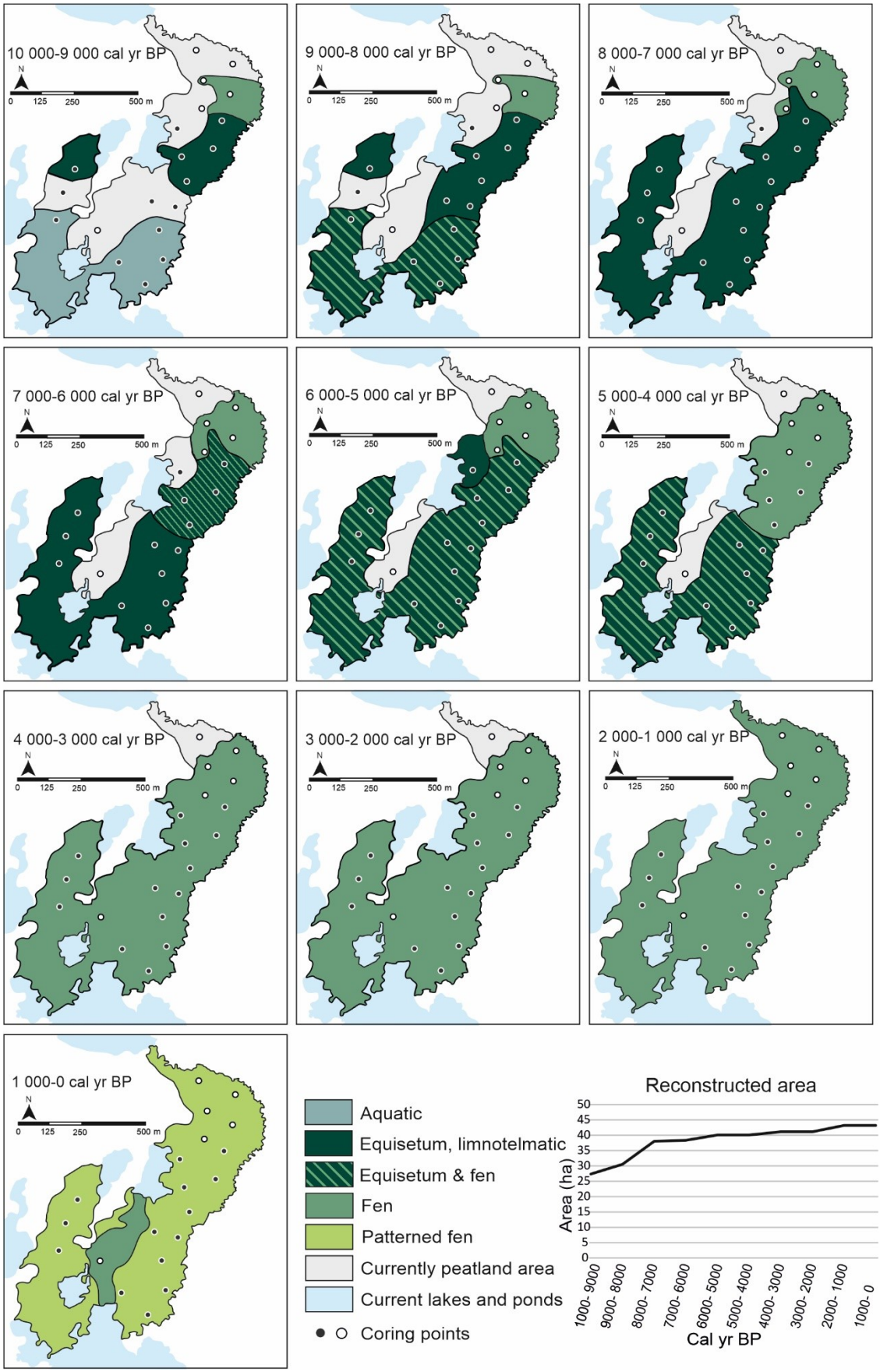
10 000-9 000 cal yr BP
9 000-8 000 cal yr BP
8 000-7 000 cal yr BP
7 000-6 000 cal yr BP
6 000-5 000 cal yr BP
5 000-4 000 cal yr BP
4 000-3 000 cal yr BP
3 000-2 000 cal yr BP
2 000-1 000 cal yr BP
1 000-0 cal yr BP
N
0 125 250 500 m
Aquatic
Equisetum, limnotelmatic
Equisetum & fen
Fen
Patterned fen
Currently peatland area
Current lakes and ponds
Coring points
Reconstructed area
Area (ha)
0 5 10 15 20 25 30 35 40 45 50
1000- 9000
9000- 8000
8000- 7000
7000- 6000
6000- 5000
5000- 4000
4000- 3000
3000- 2000
2000- 1000
1000- 0
Cal yr BP

Figure 5. Successional development of habitat distribution in patterned flark fen of Kaamanen peatland. The different colours indicate the main vegetation assemblages in thousand-year time-windows. The areas marked with grey are currently part of the peatland. Coring points with black fill indicates limnotelmatic basal conditions and white fill indicates mineral-peat transition. The graph in the bottom right corner displays the development of the reconstructed peatland area (ha) from the peatland initiation to 0 cal yr BP.

3.4 Carbon accumulation

Peat C content, measured from the short sections, was on average 47% and varied between 35% and 53% (Figure 4). The average N content was 2.2% with minimum and maximum contents of 0.9% and 3.5% (Figure 4). C and N contents were stable for the top-most 20 cm for all peat records but fluctuated more in the deeper layers (Figure 4). The diverging C content trends between the deeper sections of K1EP and K3EP was especially conspicuous, considering the close proximity of the coring sites to each other.

C accumulation was, on average, 21 and 15 g C m^{-2} yr^{-1} in the long cores STLong and EPLong, respectively. For the STLong, the CAR continuously increased from the core bottom peaking to the highest values of ca. 29 g C m^{-2} yr^{-1} between ca. 6000–7900 cal yr BP (Figure 3). A marked CAR decline of about 15 g C m^{-2} yr^{-1} was observed thereafter around 6000 cal yr BP. Only minor CAR changes were detected for the EPLong over time. However, the CAR was low: 7-8 g C m^{-2} yr^{-1} for the surface parts.

CAR varied markedly in the short surface cores, but the overall trend was mainly increasing towards the surface. In the string top cores, CAR averages were 65 g C m^{-2} yr^{-1} (K1EP) and 43 g C m^{-2} yr^{-1} (K3EP) and in the string margin cores, they were 37 g C m^{-2} yr^{-1} (K1BS) and 29 g C m^{-2} yr^{-1} (K3BS). In contrast to the long cores, CAR was highest over the recent 20 years, 210 g C m^{-2} yr^{-1} (K1BS) and ca. 100 g C m^{-2} yr^{-1} (K1EP). In K1EP core, highest values of ca. 120 g C m^{-2} yr^{-1} occurred at ca. 1100 cal yr BP (Figure 4).

3.5 Radiative forcing

While the estimated instantaneous RF varied during the peatland history, according to both flux scenarios the studied site has had a net cooling impact over the 10,000-yr period after the peatland initiation (Figures 6 and 7). This can be observed from the cumulative RF at the end of the period, which is proportional to the total additional energy in the atmosphere. In both scenarios, for the first ca. 1000 years the total (sum of CO_2 and CH_4) instantaneous RF was close to zero (Figure 7), in Scenario 1 marginally positive and in Scenario 2 negative. In Scenario 1, the total RF was positive (warming impact) approximately between 9000 and 4000 cal yr BP. The total RF turned to negative (cooling impact) after ca. 4000 cal yr

BP and reached the level of strongest cooling (ca. -10 $\times 10^{-8}$ W m^{-2}) before 1000 cal yr BP. In Scenario 2 that allowed the aquatic Sandy *Equisetum* gradually turn into a peat-forming littoral *Equisetum* vegetation, the total RF was marginally negative between ca. 10,000 and 7000 cal yr BP, close to zero between ca. 7000 and 6000 cal yr BP, and at ca. 6000 cal yr BP it turned marginally positive for ca. 400 yr. Since ca. 5500 cal yr BP, the total RF was negative, reaching the minimum of -14 $\times 10^{-8}$ W m^{-2} between ca. 1000 and 200 cal yr BP.

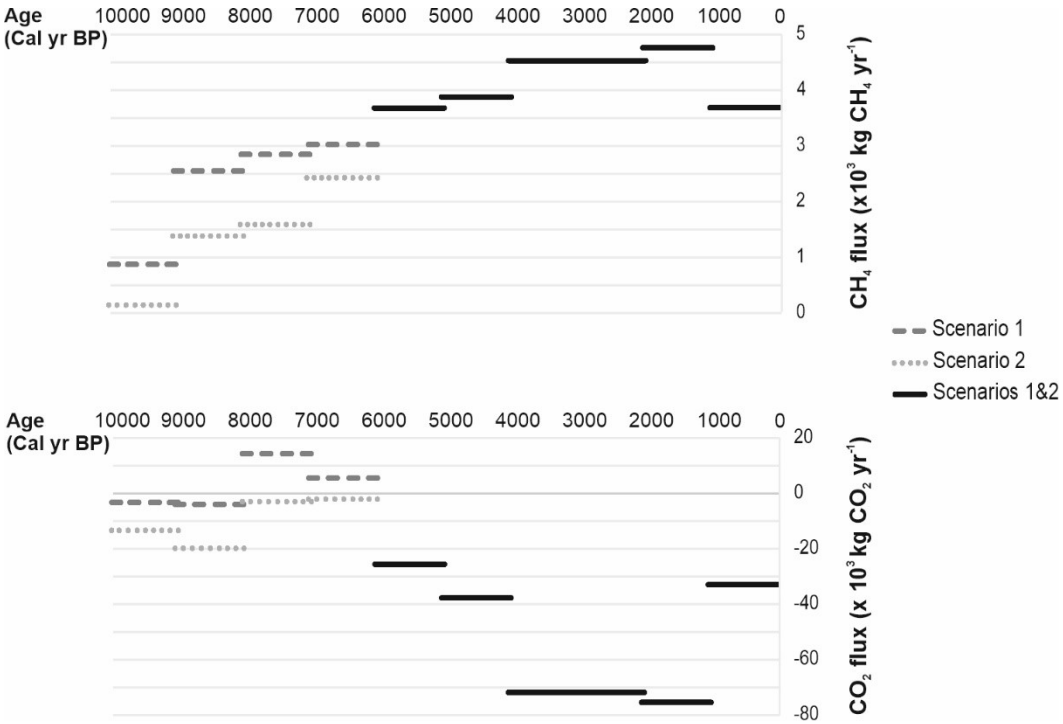

Figure 6. Reconstructed CH_4 and CO_2 flux ($\times 10^3$ kg CH_4 yr^{-1}; $\times 10^3$ kg CO_2 yr^{-1}) scenarios integrated over the total peatland area in Kaamanen peatland over time. Two alternative scenarios were created, which differ in their early development from sandy *Equisetum* habitats to peaty *Equisetum*.

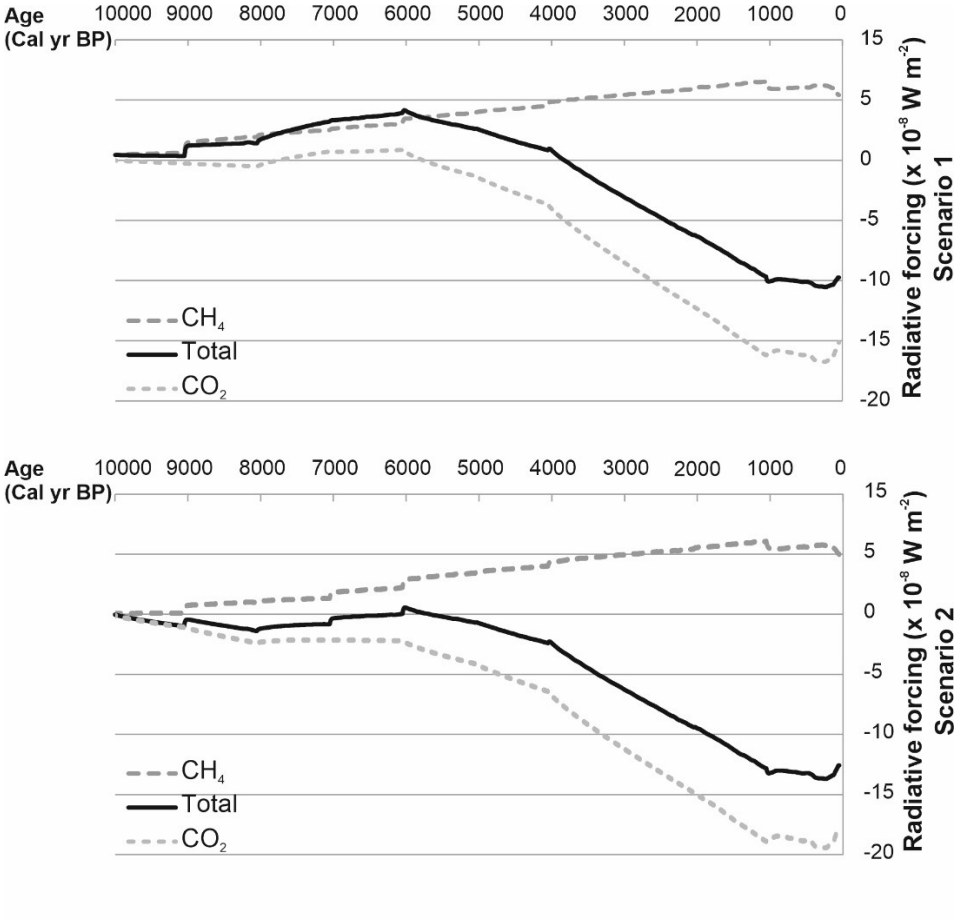

403

404 **Figure 7.** Radiative forcing (RF) due to the ecosystem-atmosphere fluxes of CO_2 and CH_4 that resulted from the
405 development of the Kaamanen peatland. Positive RF corresponds to a warming effect and negative RF to a cooling
406 effect. 'Total' RF equals the net RF due to both CO_2 and CH_4 fluxes. Scenarios 1 and 2 refer to the flux scenarios
407 shown in Fig. 6, which differ in the assumed changes within the *Equisetum* habitats.

408 **4. Discussion**

409 *4.1 Peatland initiation and development*

410 The Kaamanen area deglaciated approximately 11,000 cal yr BP (Kujansuu 1992; Kujansuu et al., 1998), which left
411 behind several melt water lakes, which were gradually filled in by organic sediments, some rapidly changing to peatlands
412 via terrestrialization. Our data suggest that the studied peatland formed soon after the ice margin withdrawal. In the
413 southern part of the peatland, open water conditions with aquatic vegetation persisted until at least approximately 9500
414 cal yr BP, after which lake infilling took place. In the middle section of the present peatland area, limnotelmatic peat with
415 abundant *Equisetum* suggests terrestrialization of the shallow littoral lake areas. In the north, peat started to form directly
416 on top of the mineral soil, as indicated by a sharp transitional contact from sand to peat. It appears that post-glacial lake
417 – stream landscape processes triggered and regulated the peatland development and expansion. The peatland development

418 in Kaamanen follows acknowledged theories (e.g. Foster and Wright Jr., 1990) of peatland formation beginning at several
419 locations, later combining into a single complex and simultaneously growing both vertically and laterally.

420 The intensive development and expansion of the studied peatland during the early Holocene agrees with earlier studies
421 from the high latitudes, which have revealed that the most rapid expansion period of peatlands occurred during ca. 10,000
422 to 8000 cal yr BP (Mäkilä and Moisanen, 2007; Weckström et al., 2010). After the rapid early Holocene paludification,
423 the lateral growth continued at a slow rate following landscape topography, including peat formation directly on mineral
424 soil. This agrees with Weckström et al. (2010), who found only modest lateral expansion from 8000 to 4000 cal yr BP.

425 Peat started to accumulate relatively simultaneously all over the studied area, but the vertical peat growth rate differed
426 greatly. The landscape is sloping from the north towards the lake in the south, and this may have created the current
427 pattern where the peat deposit thickness is 1 to 2 m in the north, while it is up to 4 m in the south. The original altitudinal
428 difference of 3 m has been evened to a 1 m difference, as the peat growth rate has been twice as high in the south as it is
429 in the north. In the northern part, measured from EPLong, the long-term average CAR of 15 g C m^2 yr^{-1} is in line with the
430 average estimated for subarctic fens in Finland, 16.9 g C m^2 yr^{-1} (Turunen et al., 2002). In the southern part, however, the
431 CAR average of 21 g C m^2 yr^{-1} from STLong is more comparable with the average accumulation of raised bogs in southern
432 Finland, 23.4 g C m^2 yr^{-1} (Turunen et al., 2002). Probably the initial infilling lake received more nutrients from the
433 surrounding catchment resulting in higher peat and C accumulation rates in the southern core (cf. Mäkilä and Moisanen
434 2007). Overall, the long-term CAR values are of the same magnitude as the mean Holocene values of northern peatlands,
435 18.6 g C m^2 yr^{-1} (Yu et al., 2009), 22.9 g C m^2 yr^{-1} (Loisel et al., 2014) and of west Siberian peatlands 17.2 6 g C m^2 yr^{-1}
436 (Turunen et al., 2011). Considerable spatial variation in the average long-term CAR within a peatland is not unprecedented
437 as suggested by studies with multiple study points (Mathijssen et al., 2017, 2016; Pelletier et al., 2017; Piilo et al., 2019;
438 Watson et al., 2015; Zhang et al., 2018a). Our data thus highlight the need for multiple study points per site, instead of
439 the common single study-point approach, to reconstruct peatland development and CAR comprehensively and properly
440 estimate basin-wide average rates.

441 *4.2 Holocene climate variations and concurrent peatland dynamics*

442 In northern Fennoscandia, **the early Holocene (ca. 11,700-8000 cal yr BP) was relatively warm** (Luoto et al., 2014;
443 Väliranta et al., 2015). In Kaamanen, during the early Holocene, the initial aquatic littoral habitat changed into a peat
444 forming *Equisetum* habitat. The CARs between 20-28 g C m^2 yr^{-1} and 12-18 C m^2 yr^{-1} determined for STLong and
445 EPLong, respectively, are in line with previous studies (Mäkilä and Moisanen, 2007; Mathijssen et al., 2014). For the
446 early limnotelmatic habitat type, we applied two CO_2 and CH_4 flux scenarios to create RF trajectories. Here, we were

447 able to apply the fluxes measured on nearby limnotelmatic *Equisetum*-dominated subarctic fen assemblages (Juutinen et
448 al., 2013), but it should be noted that only a few flux measurements from such ecosystem transitions are available and
449 this uncertainty in our assumptions needs to be taken into account when interpreting the created RF scenarios. It appeared
450 that the CO_2 and CH_4 fluxes reconstructed for the Kaamanen peatland were relatively low during the first millennium,
451 and thus both scenarios suggested a negligible RF for this period. The system was a small C sink when there were sandy
452 sediments and a net source of C to the atmosphere when organic sediments were deposited. We interpret the latter to
453 result from the release of excess C relative to the on-site C fixation, potentially due to lateral transport of organic matter
454 at the peatland-lake edge (i.e. particulate and dissolved organic C (DOC) transfer from the peatland). This results in a
455 discrepancy: peat record indicates C accumulation, while the applied C exchange rates, which we cannot retrospectively
456 verify, indicate a release of C also in the form of CO_2. This is a feature found within littoral vegetation (Larmola et al.,
457 2003) and, at a larger scale, material of terrestrial origin may turn lakes into net heterotrophic and CO_2 sources (Cole et
458 al., 1994).

459 **The Mid-Holocene (ca. 8000-5000 cal yr BP) was warm and dry** (Eronen et al., 1999; Seppä et al., 2009). The STLong
460 record showed strongly decreased C accumulation rates (from 33 to 15 g C m^2 yr^{-1}) after 6000 cal yr BP with a
461 simultaneous change from the *Equisetum* characterized assemblages to non-patterned fen vegetation. Similar mid-
462 Holocene decrease in the peat and C accumulation (from 26 to 9 g C m^2 yr^{-1}) and lateral expansion rates have been
463 detected in western Finnish Lapland (Mäkilä and Moisanen, 2007; Mathijssen et al. 2014). The RF Scenario 1, which
464 allowed the aquatic habitat to prevail only for the first 1000-yr period, showed a warming impact starting from ca. 9000
465 cal yr BP. Scenario 2, with interpolation from the sandy littoral habitat to the littoral peaty *Equisetum* peat habitat,
466 suggested a consistent cooling impact apart from a 400-yr-long period of marginal warming at around 6000 cal yr BP.
467 Our results show a notable decrease in lateral expansion already after 7000 cal yr BP, and both RF scenarios suggest that
468 the highest positive forcing took place at 6000 cal yr BP, after which RF turned to a decreasing trend, with a negative
469 forcing in Scenario 2.

470 Between 5000 and 3000 cal yr BP, i.e. in **the cooler and moister late Holocene** (Seppä and Birks, 2001), our results
471 suggest only minor changes in the vegetation, lateral expansion and CAR. Yet, the RF Scenario 1 suggests positive forcing
472 changing to negative only after 4000 cal yr BP. The overall RF pattern, however, supports the prevailing understanding
473 of a peatland ecosystem first having a warming impact, which later turns to cooling. The switchover to cooling should be
474 inevitable at some point, as part of the cooling effect due to sustained CO_2 uptake accumulates monotonously while the
475 positive RF due to a continuous CH_4 emission converges to a constant level in a few decades.

476 In contrast to the prevailing consensus and our results, the reconstructed RF of another subarctic fen, located ca. 180 km
477 southeast of our study site, suggested a slight warming effect throughout its 10,000-yr development, even though it has
478 continuously accumulated C (Mathijssen, 2016). Compared to our study site, that fen is shallower, with a maximum peat
479 depth of 2.5 m, and has a more even surface topography, it supports different (tall sedge) vegetation and differs in its
480 historical vegetation succession (Mathijssen et al., 2014). The RF scenarios for a southern Finnish boreal bog suggested
481 a positive forcing for the first 7000 yr resembling our Scenario 1, even though with a longer phase of positive forcing,
482 reflecting its long-lasting succession from a fen to a bog (Mathijssen et al., 2017).

483 While the STLong record revealed C accumulation features and changes in vegetation assemblages that seemed to reflect
484 Holocene climate variations, especially mid-Holocene decreased CAR, the other Holocene section EPLong record
485 indicated much more subtle changes in vegetation and accumulation patterns. In other words, no clear and consistent
486 peatland-scale response to warm climate was detected. However, this is possibly due to the topographic differences
487 between the two peat profiles, differences in vegetation succession, but also due to the age-depth models, of the two long
488 cores, where the compromised dating accuracy might cause inaccuracies for the results.

489 The detected vegetation succession, from *Equisetum* to Cyperaceae dominated vegetation and further to patterned fen, is
490 also reported for other northern fens (Mäkilä et al., 2001; Mäkilä and Moisanen, 2007). The formation of surface
491 microtopography with strings and flarks has been dated to the **late Holocene** 3000–2000 cal yr BP, elsewhere in Lapland
492 (Mäkilä and Moisanen, 2007; Seppälä and Koutaniemi, 1985). The current understanding is that the origin of
493 microtopography of the raised bogs and fens in Fennoscandia is probably a **large-scale cooling** of the climate and a
494 related **increase in effective humidity** (Aartolahti, 1967; Karofeld, 1998; Mäkilä and Moisanen, 2007; Seppälä and
495 Koutaniemi, 1985). The irregular string and flark pattern, now characteristic of the Kaamanen peatland, was formed only
496 after ca. 1000 cal yr BP. These formation processes were dated to both the **warm MCA** (Diaz et al., 2011; Linderholm et
497 al., 2018) and the **cool LIA** (Cook et al., 2004; Hanhijärvi et al., 2013). While the MCA and LIA temperature patterns for
498 European high-latitudes are relatively well resolved, the perception of hydrological conditions for these climate phases
499 vary more (Diaz et al., 2011; Linderholm et al., 2018). Recent peatland hydrological reconstruction for Finnish Lapland,
500 however, suggest relatively dry conditions for both periods (Zhang et al., 2018b), although these data originate from
501 permafrost peatlands, which are more complicated systems to interpret as the permafrost dynamics may complicate the
502 interpretation of hydrological changes. The dry string top in K1EP formed during the onset of the MCA at ca. 1000 cal
503 yr BP with a simultaneous decrease in CAR. However, the formation of string margin conditions in K1BS, K3BS and
504 K3EP and the following change to dry Ericales-*Pleurozium* community of K3EP occurred during the LIA. The changes
505 dated to the LIA could reflect ice- and frost-related winter processes, which cause movement of unstable landforms

506 (Koutaniemi, 1999). String formation reduced the CO_2 uptake of the fen and halted the decreasing RF trend, as CO_2
507 exchange is associated with fen microtopography and the related variability in plant communities: minerotrophic
508 communities act as effective sinks, while net CO_2 fluxes are smaller in ombrotrophic string top communities (Heikkinen
509 et al., 2002; Maanavilja et al., 2011; Heiskanen et al., 2020).

510 In our string top and string margin records, CAR was consistently low during the MCA, a pattern also reported for other
511 permafrost-influenced subarctic fens (Zhang et al., 2018a). In the string top K3EP and string margin K3BS records, CAR
512 and *Sphagnum* prevalence seemed to increase during the LIA, which contradicts previous observations of decreased CAR
513 in more southern peatlands during the LIA period (Charman et al., 2013). However, in subarctic permafrost fens higher
514 CAR was detected during the LIA corresponding to our results (Zhang et al., 2018a) and highlighting the importance of
515 *Sphagna* in peatland C dynamics by enhancing the C sink capacity (e.g. Loisel and Yu, 2013). The long records suggested
516 decreasing CARs for the LIA period, but for these two records, the chronology without ^{210}Pb dating is less reliable for the
517 recent centuries. The CARs of the past decades, including **the recent warming** since the 1980s, are high, which is at least
518 partly due to the incomplete decay process, and thus they cannot be directly compared with the older sections (Alm et al.,
519 1999; Clymo et al., 1998; Tolonen and Turunen, 1996; Young et al., 2019). However, a modelling exercise for permafrost-
520 influenced fens suggests that the recent warming has increased the peatland C sink capacity possibly through vegetation
521 changes and increased net primary productivity, even when the decomposition processes are considered (Zhang et al.,
522 2018a). High peat and C accumulation rates were also detected before the MCA for the K1EP and K1BS records (ca. 110
523 and 80 g C m^2 yr^{-1}, respectively). This pattern was not related to incomplete decay, nor especially warm climate, but
524 probably reflects a vegetation succession from a wet fen habitat to string margin (K1BS) and string top vegetation (K1EP);
525 this change was then followed by a decrease in CAR.

526 *4.3 Implications for future peatland dynamics*

527 In the future, warmer springs with earlier snowmelt will probably benefit annual CO_2 uptake of the peatland (Aurela et
528 al., 2004). However, recent ecosystem-scale field experiments have shown that, instead of a direct impact of temperature
529 *per se*, peatland water table is the major driving factor for fen CO_2 dynamics (Laine et al., 2019) and CH_4 emissions
530 (Peltoniemi et al., 2016) as well as for vegetation composition and biomass production (Mäkiranta et al., 2018). High
531 water tables support peat accumulation by maintaining anoxic conditions in the peat profile, thus slowing decomposition
532 (e.g. Belyea, 1996), while temperature and light conditions, in turn, may restrict net C accumulation (Charman et al.,
533 2013). The overall balance between gross ecosystem productivity and C loss through decomposition and DOC (Roulet et
534 al., 2007) is a complex mixture of forcing factors and, as it is also strongly influenced by site-specific characteristics, the

differentiation is challenging. Our study supports the prevailing understanding of northern peatlands acting as important long-term C sinks with climate cooling feedbacks. However, a widespread drying of European peatlands over the recent past has been suggested (Swindles et al., 2019; Zhang et al., 2020, 2018b). Water level drawdown experiments have shown that in high latitudes shrubs benefit over forbs and mosses as belowground production increases under drier conditions (Mäkiranta et al., 2018). In addition, changes in vegetation composition may occur fast: drainage of a boreal fen resulted in a rapid shift of *Carex* dominated fen vegetation to *Sphagnum* dominated ombrotrophic communities (Tahvanainen, 2011). Consequently, should the future warming be accompanied by summer water deficiency (Charman, 2007) and lowered water levels, significant changes in fen plant functional types (Mäkiranta et al., 2018) and thus in C accumulation and the related RF may occur.

5. Summary

In this study, we reconstructed peatland succession in a subarctic fen in Finland throughout the Holocene. Changes in vegetation and peat accumulation showed marked spatiotemporal differences over the studied area. The peatland started to form simultaneously on a wide area and lateral expansion was greatest during the early Holocene. Radiative forcing scenarios suggest that the net atmospheric effect of the peatland development is cooling. However, depending on the applied scenario, during the early and mid-Holocene the peatland also had a temporary warming impact due to CH_4 emissions. The current microtopography with strings and flarks formed only after ca. 1000 cal yr BP. The warm climate periods during the Holocene, did not seem to result in uniform responses in carbon accumulation rates (CAR) nor vegetation patterns, while vegetation succession in general appeared to drive changes in CAR and RF more.

6. Acknowledgements

We thank O. Kuuri-Riutta, J-P. Manner and M. Amesbury for fieldwork assistance. Academy of Finland (CAPTURE, 296423) funded this project.

7. Author contribution

MV, AK, MA, J-PT and SP designed the research. SP, LH, MV, JT, SJ, HM and MS carried out the fieldwork. SP performed the laboratory analysis under supervision from MV. J-PT, MA, E-ST and LH contributed and modelled the flux data. All authors substantially contributed to the final manuscript.

8. References

Aartolahti, T., 1967. On dating the genesis of peat banks and hollows in the raised bogs of southwestern Finland. Comptes Rendus de la Société Géologique de Finlande 39, 71–86.

Alm, J., Schulman, L., Walden, J., Nykänen, H., Martikainen, P.J., Silvola, J., 1999. Carbon balance of a Boreal bog during a year with an exceptionally dry summer. Ecology 80, 161–174. https://doi.org/https://doi.org/10.1890/0012-9658(1999)080[0161:CBOABB]2.0.CO;2

Appleby, P.G., Oldfield, F., 1978. The calculation of lead-210 dates assuming a constant rate of supply of unsupported 210 Pb to the sediment. Catena 5, 1–8.

Aurela, M., Laurila, T., Tuovinen, J.-P., 2001. Seasonal CO2 balances of a subarctic mire. J. Geophys. Res. 106, 1623–1637. https://doi.org/http://dx.doi.org/10.1029/2000JD900481; doi:10.102

Aurela, M., Laurila, T., Tuovinen, J.-P., 2004. The timing of snow melt controls the annual CO2 balance in a subarctic fen. Geophys. Res. Lett. 31, 3–6. https://doi.org/10.1029/2004GL020315

Aurela, M., Laurila, T., Tuovinen, J.-P., 2002. Annual CO2 balance of a subarctic fen in northern Europe: Importance of the wintertime efflux. J. Geophys. Res. Atmos. 107, 1–12. https://doi.org/10.1029/2002JD002055

Aurela, M., Tuovinen, J.-P., Laurila, T., 1998. Carbon dioxide exchange in a subarctic peatland ecosystem in northern Europe measured by the eddy covariance technique. J. Geophys. Res. Atmos. 103, 11289–11301. https://doi.org/10.1029/98JD00481

Belyea, L.R., 1996. Separating the Effects of Litter Quality and Microenvironment on Decomposition Rates in a Patterned Peatland. Nord. Soc. Oikos 77, 529–539.

Blaauw, M., 2010. Methods and code for "classical" age-modelling of radiocarbon sequences. Quat. Geochronol. 5, 512–518. https://doi.org/10.1016/j.quageo.2010.01.002

Blaauw, M., Christen, J.A., 2011. Flexible paleoclimate age-depth models using an autoregressive gamma process. Bayesian Anal. 6, 457–474. https://doi.org/10.1214/11-BA618

Boucher, O., Friedlingstein, P., Collins, B., Shine, K.P., 2009. The indirect global warming potential and global temperature change potential due to methane oxidation. Environ. Res. Lett. 4. https://doi.org/10.1088/1748-9326/4/4/044007

Box, J.E., Colgan, W.T., Christensen, T.R., Schmidt, N.M., Lund, M., Parmentier, F.-J.W., Brown, R., Bhatt, U.S., Euskirchen, E.S., Romanovsky, V.E., Walsh, J.E., Overland, J.E., Wang, M., Corell, R.W., Meier, W.N., Wouters, B., Mernild, S., Mård, J., Pawlak, J., Olsen, M.S., 2019. Key indicators of Arctic climate change: 1971–2017. Environ. Res. Lett. 14, 045010. https://doi.org/10.1088/1748-9326/aafc1b

Charman, D.J., Beilman, D.W., Blaauw, M., Booth, R.K., Brewer, S., Chambers, F.M., Christen, J.A., Gallego-Sala, A., Harrison, S.P., Hughes, P.D.M.M., Jackson, S.T., Korhola, A., Mauquoy, D., Mitchell, F.J.G.G., Prentice, I.C., Van Der Linden, M., De Vleeschouwer, F., Yu, Z.C., Alm, J., Bauer, I.E., Corish, Y.M.C.C., Garneau, M., Hohl, V., Huang, Y., Karofeld, E., Le Roux, G., Loisel, J., Moschen, R., Nichols, J.E., Nieminen, T.M., MacDonald, G.M., Phadtare, N.R., Rausch, N., Sillasoo, U., Swindles, G.T., Tuittila, E.S., Ukonmaanaho, L., Väliranta, M., Van Bellen, S., Van Geel, B., Vitt, D.H., Zhao, Y., 2013. Climate-related changes in peatland carbon accumulation during the last millennium. Biogeosciences 10, 929–944. https://doi.org/10.5194/bg-10-929-2013

Charman, D.J., 2007. Summer water deficit variability controls on peatland water-table changes: Implications for Holocene palaeoclimate reconstructions. Holocene 17, 217–227. https://doi.org/10.1177/0959683607075836

Clymo, A.R.S., Turunen, J., Tolonen, K., 1998. Carbon accumulation in peatland. Nord. Soc. Oikos 81, 368–388.

Cole, J.J., Caraco, N.F., Kling, G.W., Kratz, T.K., 1994. Carbon Dioxide Supersaturation in the Surface Waters of Lakes. Science (80-.). 265, 1568–1570. https://doi.org/10.1126/science.265.5178.1568 ARTICLE

Collins, M., Knutti, R., Arblaster, J., Dufresne, J.-L., Fichefet, T., Friedlingstein, P., Gao, X., Gutowski, W.J., Johns, T., Krinner, G., Shongwe, M., Tebaldi, C., Weaver, A.J., Wehner, M., 2013. Long-term Climate Change: Projections, Commitments and Irreversibility, in: Stocker, T.F., Qin, D., Plattner, G.-K., Tignor, M., Allen, S.K., Boschung, J., Nauels, A., Xia, Y., Bex, V., Midgley, P.M. (Eds.) Clim. Chang. 2013 Phys. Sci. Basis. Contrib. Work. Gr. I to Fifth Assess. Rep. Intergov. Panel Clim. Chang. Cambridge University Press, Cambridge, United Kingdom and New York, NY, USA.

608 Cook, E.R., Esper, J., Arrigo, R.D.D., 2004. Extra-tropical Northern Hemisphere land temperature variability over the
609 past 1000 years. Quat. Sci. Rev. 23, 2063–2074. https://doi.org/10.1016/j.quascirev.2004.08.013

610 Diaz, H.F., Trigo, R., Hughes, M.K., Mann, M.E., Xoplaki, E., Barriopedro, D., 2011. Spatial and temporal
611 characteristics of climate in medieval times revisited. Am. Meteorol. Soc. 92, 1487–1500.
612 https://doi.org/10.1175/2011bams-d-10-05003.1

613 Eronen, M., Hyvärinen, H., Zettenberg, P., 1999. Holocene humidity changes in northern Finnish Lapland inferred from
614 lake sediments and submerged Scots pines dated by tree-rings. The Holocene 9, 569–580.

615 Estop-Aragonés, C., Cooper, M.D.A., Fisher, J.P., Thierry, A., Garnett, M.H., Charman, D.J., Murton, J.B., Phoenix,
616 G.K., Treharne, R., Sanderson, N.K., Burn, C.R., Kokelj, S. V., Wolfe, S.A., Lewkowicz, A.G., Williams, M.,
617 Hartley, I.P., 2018. Limited release of previously-frozen C and increased new peat formation after thaw in
618 permafrost peatlands. Soil Biol. Biochem. 118, 115–129. https://doi.org/10.1016/j.soilbio.2017.12.010

619 Etminan, M., Myhre, G., Highwood, E.J., Shine, K.P., 2016. Radiative forcing of carbon dioxide, methane, and nitrous
620 oxide: A significant revision of the methane radiative forcing. Geophys. Res. Lett. 43, 614–623.
621 https://doi.org/10.1002/2016GL071930

622 Eurola, S., Bendiksen, K., Rönkä, A., 1992. Suokasviopas. 2. korjattu painos. Oulanka Reports, Viramo, J., (Eds.)
623 Oulanka Biological Station, University of Oulu, Finland

624 Foster, D.R., Wright Jr., H.E., 1990. Role of Ecosystem Development and Climate Change in Bog Formation in Central
625 Sweden. Ecology 71, 450–463.

626 Frolking, S., Roulet, N., Fuglestvedt, J., 2006. How northern peatlands influence the Earth's radiative budget: Sustained
627 methane emission versus sustained carbon sequestration. J. Geophys. Res. Biogeosciences 111, 1–10.
628 https://doi.org/10.1029/2005JG000091

629 Frolking, S., Roulet, N.T., 2007. Holocene radiative forcing impact of northern peatland carbon accumulation and
630 methane emissions. Glob. Chang. Biol. 13, 1079–1088. https://doi.org/10.1111/j.1365-2486.2007.01339.x

631 Gałka, M., Swindles, G.T., Szal, M., Fulweber, R., Feurdean, A., 2018. Response of plant communities to climate
632 change during the late Holocene: Palaeoecological insights from peatlands in the Alaskan Arctic. Ecol. Indic. 85,
633 525–536. https://doi.org/10.1016/j.ecolind.2017.10.062

634 Gong, J., Kellomäki, S., Wang, K., Zhang, C., Shurpali, N., Martikainen, P.J., 2013. Modeling CO2 and CH4 flux
635 changes in pristine peatlands of Finland under changing climate conditions. Ecol. Modell. 263, 64–80.
636 https://doi.org/10.1016/j.ecolmodel.2013.04.018

637 Gorham, E., 1991. Northern Peatlands : Role in the Carbon Cycle and Probable Responses to Climatic Warming. Ecol.
638 Appl. 1, 182–195. https://doi.org/10.2307/1941811

639 Grimm, E.C., 1991. TILIA and TILIAGRAPH Software. Springfield, Illinois.

640 Hanhijärvi, S., Tingley, M.P., Korhola, A., 2013. Pairwise comparisons to reconstruct mean temperature in the Arctic
641 Atlantic Region over the last 2 , 000 years. Clim. Dyn. 41, 2039–2060. https://doi.org/10.1007/978-1-4020-2121-
642 3

643 Hargreaves, K.J., Fowler, D., Pitcairn, C.E.R., Aurela, M., 2001. Annual methane emission from Finnish mires
644 estimated from eddy covariance campaign measurements. Theor. Appl. Climatol. 70, 203–213.
645 https://doi.org/10.1007/s007040170015

646 Heikkinen, J.E.P., Maljanen, M., Aurela, M., Hargreaves, K.J., Martikainen, P.J., 2002. Carbon dioxide and methane
647 dynamics in a sub-Arctic peatland in northern Finland. Polar Res. 21, 49–62. https://doi.org/10.1111/j.1751-
648 8369.2002.tb00066.x

649 Helbig, M., Waddington, J.M., Alekseychik, P., Amiro, B., Aurela, A., Barr, A.G., Black, T.A., Blanken, P.D., Carey,
650 S.K., Chen, J., Chi, J., Desai, A.R., Dunn, A., Euskirchen, E., Friborg, T., Flanagan, L.B., Forbrich, I., Grelle, A.,
651 Harder, S., Heliasz, M., Humphreys, E.R., Ikawa, H., Iwata, H., Isabelle, P-E., Jassal, R., Kurbatova, J.,
652 Korkiakoski, M., Kutzbach, L., Ohta, T., Lindroth, A., Ottosson, Löfvenius, M., Lohila, A., Maksimov, T.,
653 Mammarella, I., Marsh, P., Melton, J.R., Moore, P.A., Nadeau, D., Nicholls, E.M., Nilsson, M.B., Peichl, M.,
654 Petrone, R.M., Petrov, R., Quinton, W., Roulet, N., Reed, D., Runkle, B.R.K., Rutgersson, A., Sahlee, E.,
655 Sonnentag, O., Strachan, IB., Taillardat, B, Tuittila, E-S., Tuovinen, J-P., Turner, J., Ueyama, M., Varlagin, A.,
656 Wilmking, M., Wofsy, S., 2020. Increasing contribution of peatlands to boreal evapotranspiration in a warming

657 climate. Nat. Clim. Chang. https://doi.org/10.1038/s41558-020-0763-7

658 Heiri, O., Lotter, A.F., Lemcke, G., 2001. Loss on ignition as a method for estimating organic and carbonate content in
659 sediments: reproducibility and comparability of results. J. Paleolimnol. 25, 101–110.

660 Heiskanen, L., Tuovinen, J.-P., Räsänen, A., Virtanen T., Juutinen S., Penttilä, T., Linkosalmi, M., Mikola, J., Laurila,
661 T., Aurela M., 2020. Carbon dioxide and methane exchange of a patterned subarctic fen during two contrasting
662 growing seasons [Data set]. Zenodo. http://doi.org/10.5281/zenodo.3965739

663 Holmquist, J.R., Finkelstein, S.A., Garneau, M., Massa, C., Yu, Z., MacDonald, G.M., 2016. A comparison of
664 radiocarbon ages derived from bulk peat and selected plant macrofossils in basal peat cores from circum-arctic
665 peatlands. Quat. Geochronol. 31. https://doi.org/10.1016/j.quageo.2015.10.003

666 Howard, A.J., Gearey, B.R., Hill, T., Fletcher, W., Marshall, P., 2009. Fluvial sediments, correlations and
667 palaeoenvironmental reconstruction: The development of robust radiocarbon chronologies. J. Archaeol. Sci. 36,
668 2680–2688. https://doi.org/10.1016/j.jas.2009.08.006

669 IPCC, 2013. Summary for policymakers, in: Stocker, T.F., Qin, D., Plattner, G.-K., Tignor, M., Allen, S. K., Boschung,
670 J., Nauels, A., Xia, Y., Bex, V., Midgley, P.M. (Eds.), Clim. Chang. 2013 Phys. Sci. Basis. Contrib. Work. Gr. I
671 to Fifth Assess. Rep. Intergov. Panel Clim. Chang. Cambridge University Press, Cambridge, United Kingdom and
672 New York, NY, USA.

673 Jaatinen, K., Fritze, H., Laine, J., Laiho, R., 2007. Effects of short- and long-term water-level drawdown on the
674 populations and activity of aerobic decomposers in a boreal peatland. Glob. Chang. Biol. 13, 491–510.
675 https://doi.org/10.1111/j.1365-2486.2006.01312.x

676 Joos, F., Roth, R., Fuglestvedt, J.S., Peters, G.P., Enting, I.G., Von Bloh, W., Brovkin, V., Burke, E.J., Eby, M.,
677 Edwards, N.R., Friedrich, T., Frölicher, T.L., Halloran, P.R., Holden, P.B., Jones, C., Kleinen, T., Mackenzie,
678 F.T., Matsumoto, K., Meinshausen, M., Plattner, G.K., Reisinger, A., Segschneider, J., Shaffer, G., Steinacher,
679 M., Strassmann, K., Tanaka, K., Timmermann, A., Weaver, A.J., 2013. Carbon dioxide and climate impulse
680 response functions for the computation of greenhouse gas metrics: A multi-model analysis. Atmos. Chem. Phys.
681 13, 2793–2825. https://doi.org/10.5194/acp-13-2793-2013

682 Juggins, S., 2007. C2 user guide: Software for ecological and palaeoecological data analysis and visualization. Univ.
683 Newcastle, Newcastle upon Tyne, UK 1–73.

684 Juutinen, S., Väliranta, M., Kuutti, V., Laine, A.M., Virtanen, T., Seppä, H., Weckström, J., Tuittila, E.S., 2013. Short-
685 term and long-term carbon dynamics in a northern peatland-stream-lake continuum: A catchment approach. J.
686 Geophys. Res. Biogeosciences 118, 171–183. https://doi.org/10.1002/jgrg.20028

687 Karofeld, E., 1998. The dynamics of the formation and development of hollows in raised bogs in Estonia. Holocene 8,
688 697–704. https://doi.org/10.1191/095968398677584475

689 Kelly, T.J., Lawson, I.T., Roucoux, K.H., Baker, T.R., Jones, T.D., Sanderson, N.K., 2017. The vegetation history of an
690 Amazonian domed peatland. Palaeogeogr. Palaeoclimatol. Palaeoecol. 468, 129–141.
691 https://doi.org/10.1016/j.palaeo.2016.11.039

692 Köhler, P., Nehrbass-ahles, C., Schmitt, J., Stocker, T.F., Fischer, H., 2017. A 156 kyr smoothed history of the
693 atmospheric greenhouse gases CO 2 , CH 4 , and N 2 O and their radiative forcing. Earth Syst. Sci. Data 9, 363–
694 387. https://doi.org/https://doi.org/10.5194/essd-9-363-2017

695 Kokkonen, N.A.K., Laine, A.M., Laine, J., Vasander, H., Kurki, K., Gong, J., Tuittila, E., 2019. Journal of Vegetation
696 Science Responses of peatland vegetation to 15 - year water level drawdown as mediated by fertility level. J. Veg.
697 Sci. 30, 1206–1216. https://doi.org/10.1111/jvs.12794

698 Korhola, A., 1994. Radiocarbon evidence for rates of lateral expansion in raised mires in southern Finland. Quat. Res.
699 42, 299–307. https://doi.org/https://doi.org/10.1006/qres.1994.1080

700 Korhola, A., Alm, J., Tolonen, K., Jungner, H., 1996. Three-dimensional reconstruction of carbon accumulation and
701 CH4 emission during nine millennia in a raised mire. J. Quat. Sci. 11, 161–165.

702 Koutaniemi, L., 1999. Twenty-one years of string movements on the Liippasuo aapa mire, Finland. Boreas 28, 521–
703 530. https://doi.org/10.1111/j.1502-3885.1999.tb00238.x

704 Kujansuu, R., Eriksson, B., Grönlund, T., 1998. Lake Inarijarvi, northern Finland: Sedimentation and late Quaternary
705 evolution. Rep. Investig. Geol. Surv. Finl. 6–25.

706 Kujansuu, R., 1992. The deglaciation of Finnish Lapland. Geological Survey of Finland, Special Paper 15,
707 21-31.

708 Laine, A., Riutta, T., Juutinen, S., Väliranta, M., Tuittila, E.S., 2009. Acknowledging the spatial heterogeneity in
709 modelling/reconstructing carbon dioxide exchange in a northern aapa mire. Ecol. Modell. 220, 2646–2655.
710 https://doi.org/10.1016/j.ecolmodel.2009.06.047

711 Laine, A.M., Mäkiranta, P., Laiho, R., Mehtätalo, L., Penttilä, T., Korrensalo, A., Minkkinen, K., Fritze, H., Tuittila, E.-
712 S., 2019. Warming impacts on boreal fen CO 2 exchange under wet and dry conditions . Glob. Chang. Biol. 1–
713 14. https://doi.org/10.1111/gcb.14617

714 Laine, J., Harju, P., Timonen, T., Laine, A., Tuittila, E-S., Minkkinen, K., Vasander, H., 2009. The Intricate Beauty of
715 Sphagnum Mosses – A Finnish Guide to Identification. University of Helsinki Department of Forest Ecology,
716 Publications, Finland.

717 Larmola, T., Alm, J., Juutinen, S., Martikainen, P.J., Silvola, J., 2003. Ecosystem CO2 exchange and plant biomass in
718 the littoral zone of a boreal eutrophic lake. Freshw. Biol. 48, 1295–1310. https://doi.org/10.1046/j.1365-
719 2427.2003.01079.x

720 Linderholm, H.W., Nicolle, M., Francus, P., Gajewski, K., Helama, S., Korhola, A., Solomina, O., Yu, Z., Zhang, P.,
721 D'Andrea, W.J., Debret, M., Divine, D. V., Gunnarson, B.E., Loader, N.J., Massei, N., Seftigen, K., Thomas,
722 E.K., Werner, J., Andersson, S., Berntsson, A., Luoto, T.P., Nevalainen, L., Saarni, S., Väliranta, M., 2018. Arctic
723 hydroclimate variability during the last 2000 years: Current understanding and research challenges. Clim. Past 14,
724 473–514. https://doi.org/10.5194/cp-14-473-2018

725 Lohila, A., Minkkinen, K., Laine, J., Savolainen, I., Tuovinen, J.P., Korhonen, L., Laurila, T., Tietäväinen, H.,
726 Laaksonen, A., 2010. Forestation of boreal peatlands: Impacts of changing albedo and greenhouse gas fluxes on
727 radiative forcing. J. Geophys. Res. Biogeosciences 115, 1–15. https://doi.org/10.1029/2010JG001327

728 Loisel, J., Yu, Z., 2013. Recent acceleration of carbon accumulation in a boreal peatland, south central Alaska. J.
729 Geophys. Res. Biogeosciences 118, 41–53. https://doi.org/10.1029/2012JG001978

730 Loisel, J., Yu, Z., Beilman, D.W., Camill, P., Alm, J., Amesbury, M.J., Anderson, D., Andersson, S., Bochicchio, C.,
731 Barber, K., Belyea, L.R., Bunbury, J., Chambers, F.M., Charman, D.J., De Vleeschouwer, F., Fiałkiewicz-Kozieł,
732 B., Finkelstein, S.A., Gałka, M., Garneau, M., Hammarlund, D., Hinchcliffe, W., Holmquist, J., Hughes, P.,
733 Jones, M.C., Klein, E.S., Kokfelt, U., Korhola, A., Kuhry, P., Lamarre, A., Lamentowicz, M., Large, D., Lavoie,
734 M., MacDonald, G., Magnan, G., Mäkilä, M., Mallon, G., Mathijssen, P., Mauquoy, D., McCarroll, J., Moore,
735 T.R., Nichols, J., O'Reilly, B., Oksanen, P., Packalen, M., Peteet, D., Richard, P.J.H., Robinson, S., Ronkainen,
736 T., Rundgren, M., Sannel, a. B.K., Tarnocai, C., Thom, T., Tuittila, E.-S.E.S., Turetsky, M., Väliranta, M., van
737 der Linden, M., van Geel, B., van Bellen, S., Vitt, D., Zhao, Y., Zhou, W., 2014. A database and synthesis of
738 northern peatland soil properties and Holocene carbon and nitrogen accumulation. Holocene 24, 1028–1042.
739 https://doi.org/10.1177/0959683614538073

740 Luoto, T.P., Kaukolehto, M., Weckström, J., Korhola, A., Väliranta, M., 2014. New evidence of warm early-Holocene
741 summers in subarctic Finland based on an enhanced regional chironomid-based temperature calibration model.
742 Quat. Res. 81, 50–62. https://doi.org/10.1016/j.yqres.2013.09.010

743 Maanavilja, L., Riutta, T., Aurela, M., Pulkkinen, M., Laurila, T., Tuittila, E.S., 2011. Spatial variation in CO2
744 exchange at a northern aapa mire. Biogeochemistry 104, 325–345. https://doi.org/10.1007/s10533-010-9505-7

745 MacDonald, G.M., Beilman, D.W., Kremenetski, K. V., Sheng, Y., Smith, L.C., Velichko, A.A., 2006. Rapid early
746 development of circumarctic peatlands and atmospheric CH4 and CO2 variations. Science 314, 285–288.
747 https://doi.org/10.1126/science.1131722

748 Mäkilä, M., Moisanen, M., 2007. Holocene lateral expansion and carbon accumulation of Luovuoma, a northern fen in
749 Finnish Lapland. Boreas 36, 198–210. https://doi.org/10.1080/03009480600994460

750 Mäkilä, M., Saarnisto, M., Kankainen, T., 2001. Aapa Mires as a Carbon Sink and Source during the Holocene Linked
751 references are available on JSTOR for this article : Aapa mires as a carbon sink and source during the Holocene.
752 J. Ecol. 89, 589–599.

753 Mäkiranta, P., Laiho, R., Mehtätalo, L., Straková, P., Sormunen, J., Minkkinen, K., Penttilä, T., Fritze, H., Tuittila, E.S.,
754 2018. Responses of phenology and biomass production of boreal fens to climate warming under different water-
755 table level regimes. Glob. Chang. Biol. 24, 944–956. https://doi.org/10.1111/gcb.13934

Mann, M.E., Zhang, Z., Rutherford, S., Bradley, R.S., Hughes, M.K., Shindell, D., Ammann, C., Faluvegi, G., Ni, F., 2009. Global Signatures and Dynamical Origins of the Little Ice Age and Medieval Climate Anomaly. Science 326, 1256–1260. https://doi.org/10.1126/science.1166349

Mathijssen, P., Tuovinen, J.P., Lohila, A., Aurela, M., Juutinen, S., Laurila, T., Niemelä, E., Tuittila, E.S., Väliranta, M., 2014. Development, carbon accumulation, and radiative forcing of a subarctic fen over the Holocene. Holocene 24, 1156–1166. https://doi.org/10.1177/0959683614538072

Mathijssen, P.J.H., 2016. Department of Environmental Sciences Holocene Carbon Dynamics And Atmospheric Radiative Forcing of Different Types of Peatlands in Finland. Faculty of Biological and Environmental Sciences Department of Environmental Sciences University of Helsinki Finland, Helsinki, Finland.

Mathijssen, P.J.H., Kähkölä, N., Tuovinen, J.P., Lohila, A., Minkkinen, K., Laurila, T., Väliranta, M., 2017. Lateral expansion and carbon exchange of a boreal peatland in Finland resulting in 7000 years of positive radiative forcing. J. Geophys. Res. Biogeosciences 122, 562–577. https://doi.org/10.1002/2016JG003749

Mathijssen, P.J.H., Väliranta, M., Korrensalo, A., Alekseychik, P., Vesala, T., Rinne, J., Tuittila, E.S., 2016. Reconstruction of Holocene carbon dynamics in a large boreal peatland complex, southern Finland. Quat. Sci. Rev. 142, 1–15. https://doi.org/10.1016/j.quascirev.2016.04.013

Mauquoy, D., van Geel, B., 2007. Plant macrofossil methods and studies: Mire and Peat Macros. In Elias SA, editor, Encyclopedia of Quaternary Science. Amsterdam, Netherlands: Elsevier Science. p. 2315-2336. https://doi.org/10.1016/B0-44-452747-8/00229-5

McGuire, A.D., Lawrence, D.M., Koven, C., Clein, J.S., Burke, E., Chen, G., 2018. Dependence of the evolution of carbon dynamics in the northern permafrost region on the trajectory of climate change. PNAS 1–6. https://doi.org/10.1073/pnas.1719903115

Morris, P.J., Swindles, G.T., Valdes, P.J., Ivanovic, R.F., Gregoire, L.J., Smith, M.W., Tarasov, L., Haywood, A.M., Bacon, K.L., 2018. Global peatland initiation driven by regionally asynchronous warming. Proc. Natl. Acad. Sci. U. S. A. 115, 4851–4856. https://doi.org/10.1073/pnas.1717838115

Myhre, G., Shindell, D., Bréon, F.-M., Collins, W., Fuglestvedt, J., Huang, J., Koch, D., Lamarque, J.-F., Lee, D., Mendoza, B., Nakajima, T., Robock, A., Stephens, G., Takemura, T., Zhang, H., 2013. Anthropogenic and Natural Radiative Forcing, in: Stocker, T.F., Qin, D., Plattner, G.-K., Tignor, M., Allen, S.K., Boschung, J., Nauels, A., Xia, Y., Bex, V., Midgley, P.M. (Eds.) Clim. Chang. 2013 Phys. Sci. Basis. Contrib. Work. Gr. I to Fifth Assess. Rep. Intergov. Panel Clim. Chang. Cambridge University Press, Cambridge, United Kingdom and New York, NY, USA.

Nichols, J.E., Peteet, D.M., 2019. Rapid expansion of northern peatlands and doubled estimate of carbon storage. Nat. Geosci. 1–6. https://doi.org/10.1038/s41561-019-0454-z

Pelletier, N., Talbot, J., Olefeldt, D., Turetsky, M., Blodau, C., Sonnentag, O., Quinton, W.L., 2017. Influence of Holocene permafrost aggradation and thaw on the paleoecology and carbon storage of a peatland complex in northwestern Canada. The Holocene 27, 1391–1405. https://doi.org/10.1177/0959683617693899

Peltoniemi, K., Laiho, R., Juottonen, H., Bodrossy, L., Kell, D.K., Minkkinen, K., Mäkiranta, P., Mehtätalo, L., Penttilä, T., Siljanen, H.M.P., Tuittila, E., Tuomivirta, T., Fritze, H., 2016. Responses of methanogenic and methanotrophic communities to warming in varying moisture regimes of two boreal fens. Soil Biol. Biochem. 97, 144–156. https://doi.org/10.1016/j.soilbio.2016.03.007

Piilo, S.R., Zhang, H., Garneau, M., Gallego-sala, A., Amesbury, M.J., Väliranta, M.M., 2019. Recent peat and carbon accumulation following the Little Ice Age in Recent peat and carbon accumulation following the Little Ice Age in northwestern Québec , Canada. Environ. Res. Lett. 14, 75002. https://doi.org/10.1088/1748-9326/ab11ec

Pirinen, P., Simola, H., Aalto, J., Kaukoranta, J.-P., Karlsson, P., Ruuhela, R., 2012. Climatological Statistics of Finland 1981–2010., Reports 2012: Finnish Meteorological Institute.

Post, E., Alley, R., Christensen, T., Macias-Fauria, M., Forbes, B., Gooseff, M., Iler, A., Kerby, J., Laidre, K., Mann, M., Olofsson, J., Stroeve, J., Ulmer, F., Virginia, R., Wang, M., 2019. The Polar regions in a 2°C warmer world. Sci. Adv. 5, 1–13. https://doi.org/10.1126/sciadv.aaw9883

R Development Core Team, 2016. R: A Language and Environment for Statistical Computing. The R Foundation for Statistical Computing, Vienna, Austria

Räsänen, A., Juutinen, S., Tuittila, E.S., Aurela, M., Virtanen, T., 2019. Comparing ultra-high spatial resolution remote-sensing methods in mapping peatland vegetation. J. Veg. Sci. 30, 1016–1026. https://doi.org/10.1111/jvs.12769

Renssen, H., Seppä, H., Crosta, X., Goosse, H., Roche, D.M., 2012. Global characterization of the Holocene Thermal Maximum. Quat. Sci. Rev. 48, 7–19. https://doi.org/10.1016/j.quascirev.2012.05.022

Robinson, S.D., 2006. Carbon accumulation in peatlands, southwestern Northwest Territories, Canada. Can. J. Soil Sci. 86, 305–319. https://doi.org/10.4141/S05-086

Roulet, N.T., Lafleurs, P.M., Richard, P.J.H., Moore, T.R., Humphreys, E.R., Bubier, J., 2007. Contemporary carbon balance and late Holocene carbon accumulation in a northern peatland. Glob. Chang. Biol. 13, 397–411. https://doi.org/10.1111/j.1365-2486.2006.01292.x

Ruppel, M., Väliranta, M., Virtanen, T., Korhola, A., 2013. Postglacial spatiotemporal peatland initiation and lateral expansion dynamics in North America and northern Europe. Holocene 23, 1596–1606. https://doi.org/10.1177/0959683613499053

Sandmeier, K.J., 2016. ReflexW (Computer software). Sandmeier software. https://www.sandmeier-geo.de/

Sannel, A.B.K., Hempel, L., Kessler, A., Prėskienis, V., 2017. Holocene development and permafrost history in sub-arctic peatlands in Tavvavuoma, northern Sweden. Boreas. https://doi.org/10.1111/bor.12276

Seppä, H., Birks, H.J.B., 2001. July mean temperature and annual precipitation trends during the Holocene in the Fennoscandian tree-line area: Pollen-based climate reconstructions. The Holocene 11, 527–539. https://doi.org/10.1191/095968301680223486

Seppä, H., Bjune, A.E., Telford, R.J., Birks, H.J.B., Veski, S., 2009. Last nine-thousand years of temperature variability in Northern Europe. Clim. Past 5, 523–535. https://doi.org/10.5194/cp-5-523-2009

Seppälä, M., Koutaniemi, L., 1985. Formation of a string and pool topography as expressed by morphology, stratigraphy and current processes on a mire in Kuusamo, Finland. Boreas 14, 287–309. https://doi.org/10.1111/j.1502-3885.1985.tb00917.x

Swindles, G.T., Morris, P.J., Mullan, D.J., Payne, R.J., Roland, T.P., Amesbury, M.J., Lamentowicz, M., Turner, T.E., Gallego-sala, A., Sim, T., Barr, I.D., Blaauw, M., Blundell, A., Chambers, F.M., Charman, D.J., Feurdean, A., Galloway, J.M., Gałka, M., Green, S.M., Kajukało, K., Karofeld, E., Korhola, A., Lamentowicz, L., Langdon, P., Marcisz, K., Mauquoy, D., Mazei, Y.A., McKeown, M.M., Mitchell, E.A.D., Novenko, E., Plunkett, G., Roe, H. M., Schoning, K., Sillasoo, Ü., Tsyganov, A.N., van der Linden, M., Väliranta, M., Warner, B., 2019. Widespread drying of European peatlands in recent centuries. Nat. Geosci. https://doi.org/10.1038/s41561-019-0462-z

Tahvanainen, T., 2011. Abrupt ombrotrophication of a boreal aapa mire triggered by hydrological disturbance in the catchment. J. Ecol. 99, 404–415. https://doi.org/10.1111/j.1365-2745.2010.01778.x

Tolonen, K., Turunen, J., 1996. Accumulation rates of carbon in mires in Finland and implications for climate change. The Holocene 6, 171–178.

Turunen, J., Tahvanainen, T., Tolonen, K., 2001. Carbon accumulation in West Siberian mires, Russia. Global Biogeochem. Cycles 15, 285–296. https://doi.org/https://doi.org/10.1029/2000GB001312

Turunen, J., Tomppo, E., Tolonen, K., Reinikainen, A., 2002. Estimating carbon accumulation rates of undrained mires in Finland–application to boreal and subarctic regions. The Holocene 12, 69–80. https://doi.org/10.1191/0959683602hl522rp

Väliranta, M., Korhola, A., Seppä, H., Tuittila, E.S., Sarmaja-Korjonen, K., Laine, J., Alm, J., 2007. High-resolution reconstruction of wetness dynamics in a southern boreal raised bog, Finland, during the late Holocene: A quantitative approach. Holocene 17, 1093–1107. https://doi.org/10.1177/0959683607082550

Väliranta, M., Oinonen, M., Seppä, H., Korkonen, S., Juutinen, S., Tuittila, E.-S., 2014. Unexpected Problems in AMS 14C Dating of Fen Peat. Radiocarbon 56, 95–108. https://doi.org/10.2458/56.16917

Väliranta, M., Salonen, J.S., Heikkilä, M., Amon, L., Helmens, K., Klimaschewski, A., Kuhry, P., Kultti, S., Poska, A., Shala, S., Veski, S., Birks, H.H., 2015. Plant macrofossil evidence for an early onset of the Holocene summer thermal maximum in northernmost Europe. Nat. Commun. 6, 1–8. https://doi.org/10.1038/ncomms7809

Van Bellen, S., Dallaire, P.L., Garneau, M., Bergeron, Y., 2011. Quantifying spatial and temporal Holocene carbon accumulation in ombrotrophic peatlands of the Eastmain region, Quebec, Canada. Global Biogeochem. Cycles 25,

1–15. https://doi.org/10.1029/2010GB003877

Waddington, J.M., Roulet, N.T., 2000. Carbon balance of a boreal patterned peatland. Glob. Chang. Biol. 6, 87–97. https://doi.org/https://doi.org/10.1046/j.1365-2486.2000.00283.x

Watson, E.J., Swindles, G.T., Lawson, I.T., Savov, I.P., 2015. Spatial variability of tephra and carbon accumulation in a Holocene peatland. Quat. Sci. Rev. 124, 248–264. https://doi.org/10.1016/j.quascirev.2015.07.025

Weckström, J., Seppä, H., Korhola, A., 2010. Climatic influence on peatland formation and lateral expansion in sub-arctic Fennoscandia. Boreas 39, 761–769. https://doi.org/10.1111/j.1502-3885.2010.00168.x

Wilson, R., Anchukaitis, K., Briffa, K.R., Büntgen, U., Cook, E., D'Arrigo, R., Davi, N., Esper, J., Frank, D., Gunnarson, B., Hegerl, G., Helama, S., Klesse, S., Krusic, P.J., Linderholm, H.W., Myglan, V., Osborn, T.J., Rydval, M., Schneider, L., Schurer, A., Wiles, G., Zhang, P., Zorita, E., 2016. Last millennium northern hemisphere summer temperatures from tree rings: Part I: The long term context. Quat. Sci. Rev. 134, 1–18. https://doi.org/10.1016/j.quascirev.2015.12.005

Wu, J., Roulet, N.T., 2014. Climate change reduces the capacity of northern peatlands to absorb the atmospheric carbon dioxide: The different responses of bogs and fens. Global Biogeochem. Cycles 27, 1005–1024. https://doi.org/doi:10.1002/ 2014GB004845

Young, D.M., Baird, A.J., Charman, D.J., Evans, C.D., Gallego-Sala, A. V., Gill, P.J., Hughes, P.D.M., Morris, P.J., Swindles, G.T., 2019. Misinterpreting carbon accumulation rates in records from near-surface peat. Sci. Rep. 9. https://doi.org/10.1038/s41598-019-53879-8

Yu, Z., 2011. Holocene carbon flux histories of the world's peatlands: Global carbon-cycle implications. Holocene 21, 761–774. https://doi.org/10.1177/0959683610386982

Yu, Z., Beilman, D.W., Jones, M.C., 2009. Sensitivity of Northern Peatland Carbon Dynamics to Holocene Climate Change. Carbon Cycl. North. Peatlands 55–69. https://doi.org/10.1029/2008GM000822

Yu, Z., Loisel, J., Brosseau, D.P., Beilman, D.W., Hunt, S.J., 2010. Global peatland dynamics since the Last Glacial Maximum. Geophys. Res. Lett. 37, 1–5. https://doi.org/10.1029/2010GL043584

Zhang, H., Gallego-Sala, A. V., Amesbury, M.J., Charman, D.J., Piilo, S.R., Väliranta, M.M., 2018a. Inconsistent Response of Arctic Permafrost Peatland Carbon Accumulation to Warm Climate Phases. Global Biogeochem. Cycles 1605–1620. https://doi.org/10.1029/2018GB005980

Zhang, H., Piilo, S.R., Amesbury, M.J., Charman, D.J., Gallego-Sala, A. V., Väliranta, M.M., 2018b. The role of climate change in regulating Arctic permafrost peatland hydrological and vegetation change over the last millennium. Quat. Sci. Rev. 182, 121–130. https://doi.org/10.1016/j.quascirev.2018.01.003

Zhang, H., Väliranta, M., Piilo, S., Amesbury, M.J., Aquino-López, M.A., Roland, T.P., Salminen-Paatero, S., Paatero, J., Lohila, A., Tuittila, E., 2020. Decreased carbon accumulation feedback driven by climate-induced drying of two southern boreal bogs over recent centuries. Glob. Chang. Biol. 1–14. https://doi.org/10.1111/gcb.15005